quantum reports

MDPI

Article

Quantum Image Representation with Enhanced Intensity Preservation and Fidelity (IP-QIR)

Vrushali Nikam [1,*], Shirish Sane [2] and Manish Motghare [3]

[1] MET Institute of Engineering, Bhujbal Knowledge City, Nashik 422003, India
[2] Gokhale Education Society's R. H. Sapat College of Engineering, Management Studies and Research, Nashik 422005, India; principal@ges-coengg.org
[3] Suvidha Foundation, Nagpur 441102, India; motgharemanish@gmail.com
* Correspondence: vrushali.nikam@ges-coengg.org

Abstract

Quantum image representation (QIR) is the basic idea behind quantum image processing. It explains how a normal image is converted into quantum states so that it can be processed using quantum computers. The commonly used models for QIR are Flexible Representation of Quantum Images (FRQIs) and Novel Enhanced Quantum Representation (NEQR). Though these approaches highlight the potential of quantum-based image encoding, the limitation of practical applicability on Noisy Intermediate-Scale Quantum (NISQ) devices exists. In this paper, we propose an intensity-preserving quantum image representation (IP-QIR) scheme that aims to maintain accurate grayscale intensity information while significantly reducing quantum resource usage. The proposed method employs a controlled rotation-based encoding strategy, where pixel intensities are embedded into the measurement probability of a single intensity qubit, and spatial information is represented using position qubits. To further enhance feasibility on near-term quantum hardware, the framework operates on small image patches instead of full-resolution images, thereby reducing circuit depth and overall complexity. The performance of the proposed IP-QIR approach is evaluated through IBM Qiskit simulations on three types of grayscale images: synthetic image patches, synthetic aperture radar (SAR) images, and medical tuberculosis (TB) chest X-ray images. Experimental results demonstrate that IP-QIR achieves better intensity preservation than FRQIs and NEQR, with fidelity values reaching up to 84.12% for both SAR and medical datasets. In addition, IP-QIR represents a 4×4 image patch using only five qubits, which significantly reduces the qubit requirement when compared to NEQR, while still preserving high reconstruction accuracy.

Keywords: IBM qiskit; image fidelity; intensity preservation; intensity-preserving QIR (IP-QIR); noisy intermediate-scale quantum (NISQ); quantum image representation

Check for updates

Academic Editor: Michel Planat

Received: 28 February 2026
Revised: 6 April 2026
Accepted: 14 April 2026
Published: 22 April 2026

Copyright: © 2026 by the authors. Licensee MDPI, Basel, Switzerland. This article is an open access article distributed under the terms and conditions of the Creative Commons Attribution (CC BY) license.

1. Introduction

Quantum computing is creating new ways to handle and analyze visual information. One important challenge is how to represent regular (classical) images on a quantum computer. Quantum image representation (QIR) methods do this by encoding both pixel intensities and their positions into quantum states. Quantum image representation methods have been widely studied [1–5]. This allows image processing and analysis to be carried out directly in the quantum domain. QIR is especially relevant in areas like medical imaging, remote sensing, and synthetic image analysis, where keeping intensity details

accurate, reconstructing images reliably, and using computational resources efficiently are all critical [6–10].

Over the years, several QIR approaches have been developed. Flexible Representation of Quantum Images (FRQIs) encodes pixel positions and grayscale intensities using amplitude-based rotations, providing a compact representation that uses relatively few qubits [11–15]. On the other hand, Novel Enhanced Quantum Representation (NEQR) uses basis-state encoding for pixel intensities, which allows exact intensity representation but at the cost of higher qubit usage and more complex gate structures. Although both techniques show the possibilities of image encoding with quantum, they are not without limitations. The probabilistic amplitude measurements provided by FRQIs may cause slight deviations in pixel intensities and would be sensitive to noise. NEQR is theoretically a more accurate circuit that only needs a larger number of qubits, taking a more circuitous path and is therefore difficult to realize on a near-term quantum computer [16–20].

In particular, precise pixel intensity is of great interest in such applications as synthetic aperture radar (SAR) and medical diagnostics. SAR images frequently have fine textual and structural content, which is essential to their interpretation and analysis. Similarly, in medical imaging, such as chest X-rays for tuberculosis diagnosis, even small variations in intensity can indicate important clinical features. Any errors in reconstruction due to quantum encoding could therefore reduce the usefulness of these images for further analysis [21–25].

Figure 1 illustrates the limitations of conventional quantum image representation techniques and the motivation behind the proposed IP-QIR approach.To address these challenges, we propose a new intensity-preserving quantum image representation (IP-QIR) framework. The main idea is to encode pixel intensities with high accuracy while keeping quantum resource usage and circuit complexity low. In IP-QIR, intensity values are mapped to the measurement probability of a single intensity qubit, while position qubits capture spatial information. Moreover, the method works on small image patches instead of entire images. This patch-based strategy reduces qubit requirements and circuit depth, making the approach suitable for current Noisy Intermediate-Scale Quantum (NISQ) devices [26–38].

We evaluated IP-QIR using IBM Qiskit simulations across three types of grayscale images: (i) synthetic image patches with controlled patterns for baseline evaluation [39,40], (ii) SAR images with high-frequency structures and realistic noise patterns and (iii) medical tuberculosis (TB) chest X-ray patches, where subtle intensity differences are important for accurate diagnosis. Results show that IP-QIR consistently improves intensity preservation and encoding efficiency compared to FRQIs and NEQR while requiring fewer qubits [41–50].Overall, the method achieves a good balance between accuracy and resource efficiency [51–55].

The key contributions of this work are summarized as follows:

1. The proposal of the IP-QIR architecture for high-fidelity, intensity-preserving quantum image representation.
2. A comparative analysis of IP-QIR, FRQIs and NEQR on synthetic and SAR data and medical data.
3. A patch-based encoding approach that scales back on the use of qubits and circuit depth and is, thus, feasible with NISQ devices.
4. Large-scale experiments with evaluation based on metrics as indicators of logic size, circuit depth, encoding efficiency, pixel fidelity, and information preservation.

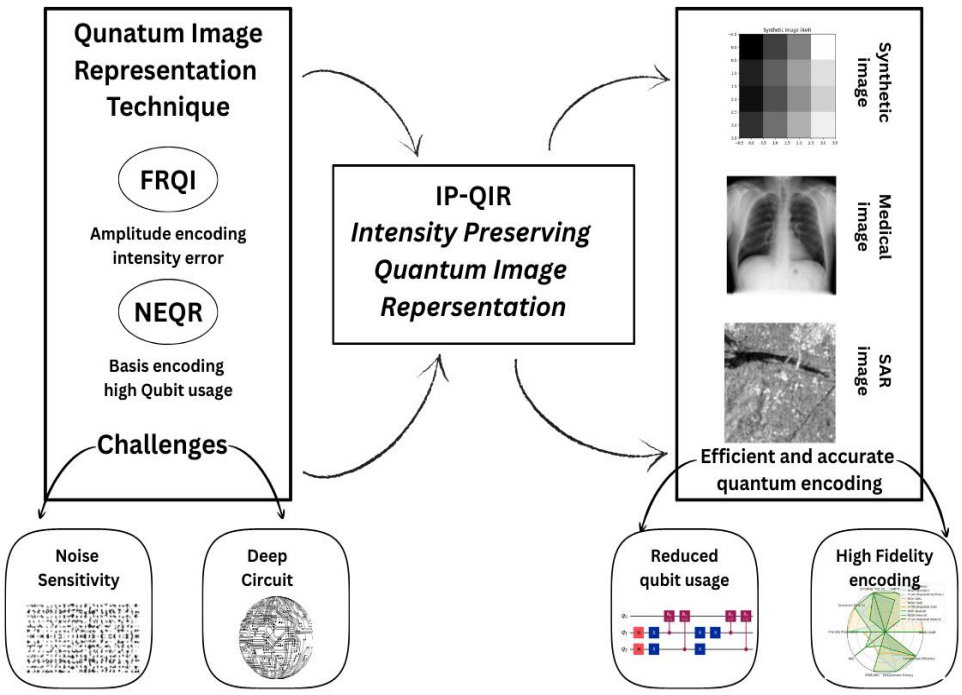


Figure 1. Limitations of conventional quantum image representation techniques, namely FRQI and NEQR, and the motivation for the proposed Intensity Preserving Quantum Image Representation (IP-QIR) approach. The figure highlights challenges such as noise sensitivity and deep circuit complexity, and demonstrates how IP-QIR enables efficient and accurate quantum encoding with reduced qubit usage and high-fidelity reconstruction for synthetic, medical chest X-ray, and SAR images.

This paper is organized into the following sections. Section 2 presents the motivation and background of this study, and the problem statement is given in Section 3. The research gap is pointed out by reviewing the current quantum image representation techniques in Section 4 of this paper. The IP-QIR approach is presented in Section 5. Section 6 provides the datasets and the preprocessing processes. Section 9 gives the details of the experimental setup and its implementation, and the evaluation criteria are found in Section 10. The results and analysis will be delivered in Section 11, and conclusions and future directions are given in Section 12.

2. Motivation

Quantum image processing is a current field that represents an efficient way of representing and processing visual information on quantum platforms. Although classical image processing methods are mature, they have serious issues regarding scalability and parallelism—factors that are relied upon in the handling of massive data or high numbers of dimensions. Current approaches to quantum image representation, including FRQIs [16,17] and NEQR [9,10], provide pathways to leverage quantum advantages but encounter critical trade-offs between pixel intensity fidelity, qubit requirements, and circuit complexity [6,15].

Such trade-offs are particularly relevant in Noisy Intermediate-Scale Quantum (NISQ) systems, where limitations in qubit count, circuit depth, and coherence time must be carefully balanced [22,23]. It is especially important that intensity representation should be represented correctly because slight deviations may result in the distortion of essential information in medical imaging and remote sensor use, among others; this can happen due to even minor deviations in the intensity representation [56–60]. In the meantime, extremely high usages of qubits or circuits can make techniques in practice invalid regarding real-world NISQ-era devices [61–65].

The consideration behind this work is the necessity to implement a quantum image representation scheme that is able to maintain pixel intensity at a high fidelity and optimally utilize quantum resources. Using patch-based encoding and an effective controlled rotation gate, the proposed IP-QIR architecture overcomes the shortcomings of the available formulations. This will enable quantum image processing to be more abundant and robust against imprecision in the sensitive area of application [66–70].

3. Problem Statement

Quantum image representation techniques are problematic in terms of high-resolution image processing in medical imaging and remote sensing, among others. Full-resolution images are commonly the focus of classical quantum image models (FRQIs and NEQR) that, as a consequence, demand too many qubits and complicated quantum circuits. These properties complicate their practical execution for both modern quantum simulators and near-term quantum machines.

The FRQIs approach represents pixel encoding using a single qubit with rotation angles, and this results in probabilistic reconstruction as well as the possible loss of precise intensity information. NEQR offers a more accurate representation of intensity via the encoded pixel values of the computational basis, but it is highly inefficient and consumes a lot of qubits and circuit depth. Other techniques, such as MCQI, GQIR, FTQR, and QUALPI, strive to meet the needs of resource efficiency and resource fidelity but are inapplicable to large-scale, realistic data, such as in medical scans or SAR images, because of scalability constraints.

In order to overcome these issues, this paper suggests a patch-based intensity-preserving quantum image representation (IP-QIR) system. The algorithm has been used to cut images into small patches, which reduces the requirements of the qubits and complexity of the circuits while still being able to access all the pixels with accurate intensity information. Such a method enables the analytical encoding (along with decoding) of synthetic, SAR, and characterized image patches, enabling quantum picture handling to be realistic regarding real-world information, and does not infringe on fidelity.

The primary objectives of the IP-QIR model are:

1. Intensity Preservation: Ensuring that pixel intensity values are accurately represented and reconstructed.
2. Resource Efficiency: Minimizing qubit usage and circuit depth, making simulations practical on current quantum platforms.
3. Scalability: Enabling the processing of real-world image datasets by focusing on smaller patches rather than full images.

IP-QIR overcomes the drawbacks of current quantum image representations, which allows a viable and efficient scheme for the high-fidelity quantum encoding of complex images. This opens the door to real-world applications in terms of medical imaging and remote sensing.

Research Gaps and Future Directions

Regardless of all the regular advancements in quantum image representation (QIR) models, a trade-off still exists between intensity fidelity and quantum resource efficacy. Probabilistic methods, including FRQI [1], have low qubit costs and shallow circuit depth but introduce intensive distortion on their reconstruction, which restricts their usefulness in precision-sensitive imaging actions. NEQR-type deterministic models such as NEQR [4] give perfect preservation of intensity. Nevertheless, a high qubit count and deep circuits mean that they can only scale to larger images and be practically deployed on NISQ-era quantum devices.

Although multi-channel and enhanced versions, such as MCQI and EFRQI/QRCI [2,3], aim to strike a compromise between fidelity and resource consumption, they continue to experience severe resource-encoding challenges on large or real-world images. Moreover, the majority of the available approaches are centered around full-image description, and, consequently, this increases circuit depth, restricting the feasibility of simulation and hardware modeling [10,11,15,18,19].

These drawbacks underline the necessity to implement a model of quantum image representation that would be able to retain pixel intensities without errors and, at the same time, become resource-efficient and scalable. By taking advantage of patch-based encoding, intensity-preserving quantum image representation (IP-QIR) is proposed to meet an intensive test goal regarding mitigating qubit usage and manageable circuit depth, matching the exact challenge posed against dynamically affected physical datasets such as synthetic images, SAR pictures, and medical images [71–76].

Furthermore, there is limited exploration of hybrid classical quantum strategies that could dynamically optimize encoding based on image content complexity. The absence of standardized benchmarking protocols and real-world validation also makes it difficult to fairly compare different QIR models. These gaps indicate a pressing need for more robust, adaptive, and experimentally viable approaches that can bridge the divide between theoretical efficiency and practical deployment in quantum imaging systems [77–82]. Recent advancements in quantum image representation and intelligent monitoring systems highlight significant progress, yet several research gaps remain. Emerging models such as QIPC and multidimensional quantum pixel representations have improved encoding flexibility and scalability; however, challenges related to noise resilience, hardware constraints, and efficient real-time implementation persist [83,84]. Similarly, quantum-inspired and hybrid deep learning frameworks for image classification demonstrate enhanced performance, but often lack interpretability and require high computational resources [85,86]. In parallel, pipeline monitoring and fault detection systems leveraging neural networks and deep learning have shown promising accuracy, though issues such as generalization across diverse environments, robustness to complex intrusion patterns, and integration with quantum-enhanced techniques are still underexplored [87–89]. Future research should therefore focus on developing hybrid quantum classical architectures with improved robustness, reduced circuit complexity, and domain-specific adaptability, enabling practical deployment in real world large scale imaging and monitoring applications.

4. Related Work

Quantum image representation (QIR) offers a mathematical theory to encapsulate classical information about images into the quantum state, thus making the quantum processing operations of storage, transmission and manipulation of quantum images possible [1–4]. Over the past two decades, several QIR models have been proposed, each differing in how pixel position and intensity information are encoded onto quantum registers. These representations exhibit inherent trade-offs among qubit efficiency, circuit depth, reconstruction fidelity, and scalability [1,5–7,9].

To provide a clear overview of these techniques and their relationships, Figure 2 presents a professional taxonomy of major QIR methods. The figure groups techniques into three categories: spatial-domain methods, which primarily encode images using amplitude or basis states (e.g., FRQI [16,17], NEQR [5,9], MCQI [20], GQIR [14]); specialized/enhanced methods, which incorporate frequency-domain, compressed, multi-wavelength, or structure-aware approaches (e.g., FTQR [5,12], QUALPI [3,13], QRMW [3,21], EBA-QR/SA-QIR [3,40]); and enhanced variants, which refine amplitude encoding strategies for improved fidelity and expressiveness (e.g., EFRQI [3,16], QRCI [3,15]). This hierarchical organization highlights

both the evolution and the inherent trade-offs of existing QIR techniques, providing readers with a concise visual summary before delving into detailed descriptions.

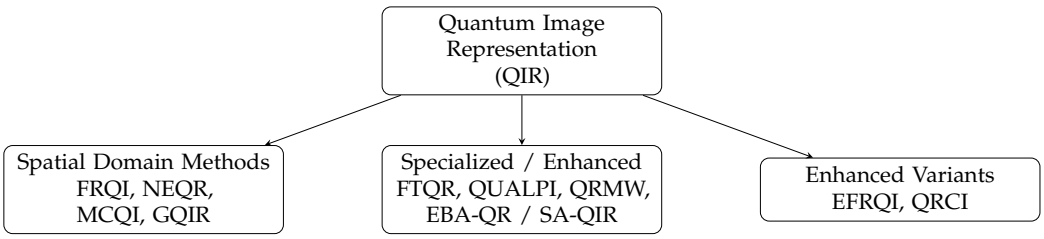


Figure 2. Quantum image representation (QIR) techniques—A professional taxonomy. The tree shows spatial-domain, specialized/enhanced and enhanced variant methods.

4.1. Flexible Representation of Quantum Images (FRQIs)

The flexible representation of quantum images (FRQIs) encodes grayscale images by mapping pixel intensity information onto the probability amplitudes of a single color qubit, while spatial coordinates are represented using position qubits [15–17]. The FRQIs state is defined as shown in Equation (1).

$$|\Psi_{\text{FRQI}}\rangle = \frac{1}{2^n}\sum_{x=0}^{2^n-1}\sum_{y=0}^{2^n-1}\left(\cos\theta_{x,y}|0\rangle + \sin\theta_{x,y}|1\rangle\right)|x,y\rangle \tag{1}$$

where $\theta_{x,y} \in [0, \pi/2]$ denotes the normalized grayscale intensity of the pixel at position (x, y).

The FRQIs approach is highly qubit-efficient and supports relatively shallow quantum circuits, making it attractive for early-stage quantum implementations [15,16]. However, its probabilistic measurement mechanism causes intensity distortion during image reconstruction, which limits its applicability in domains requiring precise pixel-level fidelity [12,15].

4.2. Novel Enhanced Quantum Representation (NEQR)

Novel Enhanced Quantum Representation (NEQR) addresses the probabilistic limitation of FRQIs by encoding pixel intensity values directly into the computational basis states [1,7,9]. The corresponding quantum image state is given in Equation (2).

$$|\Psi_{\text{NEQR}}\rangle = \frac{1}{2^n}\sum_{x=0}^{2^n-1}\sum_{y=0}^{2^n-1}|I_{x,y}\rangle \otimes |x,y\rangle \tag{2}$$

where $|I_{x,y}\rangle$ represents the binary-encoded grayscale intensity of the pixel at position (x, y).

NEQR enables deterministic image reconstruction with exact intensity preservation, making it suitable for accuracy-critical applications [7,9]. However, this benefit comes at the cost of increased qubit requirements and deeper circuits, significantly limiting its scalability and feasibility on Noisy Intermediate-Scale Quantum (NISQ) devices [2].

4.3. Multi-Channel Quantum Image Representation (MCQI)

Multi-Channel Quantum Image (MCQI) representation extends FRQIs to support color images by encoding RGB intensity components into multiple color qubits [2,7]. The MCQI quantum state is expressed in Equation (3).

$$\begin{aligned}|\Psi_{\text{MCQI}}\rangle = \frac{1}{2^n}\sum_{x,y}\Big(&\left(\cos\theta^R_{x,y}|0\rangle + \sin\theta^R_{x,y}|1\rangle\right)\\ &\otimes\left(\cos\theta^G_{x,y}|0\rangle + \sin\theta^G_{x,y}|1\rangle\right)\\ &\otimes\left(\cos\theta^B_{x,y}|0\rangle + \sin\theta^B_{x,y}|1\rangle\right)\Big)\otimes|x,y\rangle\end{aligned} \tag{3}$$

MCQI improves color expressiveness and supports richer visual information. However, the use of multiple color qubits significantly increases circuit depth and quantum

resource consumption, which constrains its practical deployment on current quantum hardware [2].

4.4. Generalized Quantum Image Representation (GQIR)

Generalized quantum image representation (GQIR) supports flexible image dimensions and arbitrary intensity ranges within a unified quantum framework [2]. Unlike fixed-dimension representations, GQIR enables scalable encoding by jointly representing pixel position and intensity information. The quantum image state in GQIR is formulated in Equation (4)

$$|\Psi_{\mathrm{GQIR}}\rangle = \frac{1}{\sqrt{N}} \sum_{k=0}^{N-1} |P_k\rangle \otimes |I_k\rangle \tag{4}$$

where $|P_k\rangle$ denotes the quantum state corresponding to the pixel position, and $|I_k\rangle$ represents the associated pixel intensity.

Although GQIR provides enhanced flexibility compared to earlier QIR models, it is susceptible to phase accumulation and coherence-related errors as image size increases, potentially reducing reconstruction fidelity and limiting robustness on NISQ-era devices [2].

4.5. Fourier Transform-Based Quantum Representation (FTQR)

Fourier Transform-Based Quantum Representation (FTQR) encodes image information in the frequency domain by applying Quantum Fourier Transform (QFT) to a spatial-domain quantum image state [2,7]. This transformation enables efficient representation of spectral components and supports frequency-domain image analysis.

The FTQR quantum image state is expressed as

$$|\Psi_{\mathrm{FTQR}}\rangle = \mathrm{QFT}\Big(|\Psi_{\mathrm{spatial}}\rangle\Big) \tag{5}$$

where $|\Psi_{\mathrm{spatial}}\rangle$ represents the quantum state of the image in the spatial domain.

FTQR is particularly effective for spectral filtering and frequency-based processing tasks. However, the transformation results in a loss of direct spatial locality, complicating pixel-wise operations and precise spatial reconstruction, which limits its suitability for applications requiring exact intensity preservation [2,3].

4.6. Quantum Image Lossless Processing Interface (QUALPI)

Quantum Image Lossless Processing Interface (QUALPI) aims to minimize qubit usage by compressing pixel intensity information into compact quantum states, thereby improving storage efficiency in quantum image representations [2,15]. Spatial information is preserved through position qubits, while intensity values are encoded in a reduced form.

The QUALPI quantum image state can be expressed as

$$|\Psi_{\mathrm{QUALPI}}\rangle = \sum_i \alpha_i |P_i\rangle \otimes |C_i\rangle \tag{6}$$

where $|P_i\rangle$ represents pixel position states, and $|C_i\rangle$ denotes compressed intensity information. While QUALPI achieves improved qubit efficiency compared to exact encoding schemes, the compression mechanism can lead to information loss during reconstruction, resulting in reduced intensity fidelity and limiting its applicability in precision-critical imaging tasks [3,15].

4.7. Quantum Representation of Multi-Wavelength Images (QRMW)

Quantum Representation of Multi-Wavelength Images (QRMW) extends quantum image encoding to multispectral and multi-wavelength data by jointly representing spa-

tial coordinates, wavelength information, and pixel intensities within a unified quantum state [2,3,7]. This representation is particularly suited for applications involving hyperspectral imaging and remote sensing.

The QRMW quantum image state is expressed as

$$|\Psi_{\text{QRMW}}\rangle = \sum_{x,y,\lambda} |I_{x,y,\lambda}\rangle \otimes |x,y\rangle \otimes |\lambda\rangle \tag{7}$$

where $|I_{x,y,\lambda}\rangle$ denotes the intensity value corresponding to spatial position (x,y) and wavelength λ. Although QRMW enables rich spectral analysis and supports advanced imaging modalities, it requires additional quantum registers and controlled operations, leading to increased qubit overhead and circuit depth. These requirements limit its scalability and practical deployment on Noisy Intermediate-Scale Quantum (NISQ) devices [2,3].

4.8. Entropy-Based and Structure-Aware Representations (EBA-QR & SA-QIR)

Entropy-Based Quantum Representation (EBA-QR) and Structure-Aware Quantum Image Representation (SA-QIR) focus on preserving the statistical distributions and structural characteristics of images rather than exact pixel-wise intensity values [2,3,8]. These approaches aim to capture global image information such as texture, entropy, or structural patterns that are relevant for high-level analysis.

Entropy is commonly used as a quantitative measure and is defined as

$$H = -\sum p_i \log_2 p_i \tag{8}$$

where p_i denotes the probability associated with the i-th pixel or feature component [2]. While such representations are effective for feature-driven tasks, including pattern recognition and structural analysis, they typically introduce additional circuit complexity and do not support precise intensity reconstruction, limiting their applicability in general-purpose and precision-critical quantum imaging applications [3].

4.9. Enhanced FRQIs Variants (EFRQI)

Enhanced Flexible Representation of Quantum Images (EFRQIs) and related variants, such as Quantum Representation of Color Images (QRCIs), extend the original FRQIs framework by introducing refined amplitude encoding strategies to improve the expressiveness of pixel intensity representation while maintaining low qubit requirements [2,3].

$$|\Psi_{\text{EFRQI}}\rangle = \sum_{x,y} (\alpha_{x,y}|0\rangle + \beta_{x,y}|1\rangle)|x,y\rangle \tag{9}$$

In this formulation, $\alpha_{x,y}$ and $\beta_{x,y}$ are functions of the normalized pixel intensity at position (x,y). These variants aim to reduce intensity distortion and enhance visual quality compared to FRQI [2]. However, since intensity information remains encoded in probability amplitudes, the reconstruction process is still probabilistic, resulting in residual intensity degradation and limiting their suitability for precision-critical imaging applications [3].

4.10. Recent Advances in Image Processing and Their Relevance to IP-QIR

Recent advances in quantum image representation, including hybrid and compression-based approaches, are directly relevant to the proposed IP-QIR framework. Unlike prior methods, IP-QIR explicitly integrates intensity-driven parameterization with scalable circuit design [87–89].

5. Proposed Method: Intensity-Preserving Quantum Image Representation (IP-QIR)

Here, we present the proposed intensity-preserving quantum image representation (IP-QIR), a quantum image encoding model that helps to address the key challenges of current quantum image representation methods, i.e., probabilistic encoding of intensity, excessive use of qubits, and large circuit depth. The main goal of IP-QIR is to achieve efficient preservation of pixel intensity data at the cost of a limited amount of resources, and thus, it can be implemented in practice on Noisy Intermediate-Scale Quantum (NISQ) devices.

In contrast to the traditional methods of encoding, which involve amplitude or basis-state-based encoding, IP-QIR uses a hybrid encoding approach where grayscale data is retained via the controlled value of an amplitude, and fewer qubits, along with moderate circuit complexity, are used. This architecture renders IP-QIR applicable to real-world image data, such as synthetic, SAR and medical images. The proposed intensity-preserving quantum image representation (IP-QIR) framework introduces a fundamentally different hybrid encoding strategy compared to existing quantum image representations such as FRQI, NEQR, and EFRQI. Traditional approaches primarily rely on a single encoding paradigm—either amplitude-based encoding (e.g., FRQI/EFRQI) or basis-state encoding (e.g., NEQR). Although amplitude encoding is compact, it often suffers from indirect intensity retrieval and sensitivity to noise, whereas basis encoding provides exact intensity values at the cost of increased qubit requirements.

In contrast, the proposed IP-QIR framework adopts a hybrid encoding mechanism that integrates the advantages of both paradigms. Specifically, it preserves pixel intensity information through structured encoding while simultaneously enabling compact representation using controlled amplitude modulation. This hybridization ensures that intensity information is neither fully embedded in fragile amplitudes nor entirely dependent on qubit-heavy basis states.

Furthermore, unlike EFRQI-based methods that focus primarily on amplitude refinement, IP-QIR introduces an intensity-preserving transformation that maintains a direct correspondence between encoded quantum states and original pixel values. This improves interpretability, reconstruction fidelity, and robustness under practical constraints such as NISQ noise.

Therefore, the novelty of IP-QIR lies in its balanced trade-off between representation efficiency, intensity preservation, and implementation feasibility, distinguishing it from existing quantum image representation techniques.

5.1. Formal Classification of IP-QIR

The proposed IP-QIR framework belongs to the class of amplitude-encoded quantum image representations, similar to FRQIs and EFRQIs. However, unlike FRQIs, which encodes pixel intensities via global rotation angles applied uniformly across superposed position states, IP-QIR introduces a hybrid encoding strategy where intensity-dependent amplitudes are locally parameterized.

- **FRQIs:** Global rotation encoding, depth $\mathcal{O}(N^2)$;
- **EFRQI:** Optimized rotation with compression;
- **IP-QIR:** Hybrid amplitude encoding with structured state preparation.

Admissible Operations: IP-QIR supports controlled rotations and local unitary transformations, enabling compatibility with NISQ-limited gate sets.

5.2. Overview of the Proposed IP-QIR Method

The IP-QIR channel processes grayscale images in a quantum system, which impressively describes the coordinates of pixel location and intensity by using dual control quantum interaction. The overall process of encoding takes the following steps:

1. Image Preprocessing Scaling: The quantum register necessities are converted to the required input dimension of $2^n \times 2^n$. The pixels are vacuumed to the scale of $[0, 1]$ to enable encoding using amplitude.
2. Intensity Mapping: Apply each normalized pixel intensity to a rotation angle, which settles the chance amplitudes of the intensive qubit.
3. Quantum Circuit Construction: A quantum circuit is built by adding position qubits with one intensity qubit, with the rotational gates being generalized to multi-controlled, updating intensities as needed, based on the spatial coordinates of a pixel.
4. Quantum Simulation and Measurement: The quantum simulator, which is the IBM Qiskit quantum simulator, is used to simulate the built circuit, and statistical measurements are taken.
5. Image Reconstruction and Evaluation: The original image is constructed using the results of the measurements, and performance measurements, including fidelity, information loss, and circuit complexity, are calculated.

The overall workflow of the proposed IP-QIR framework is illustrated in Figure 3.

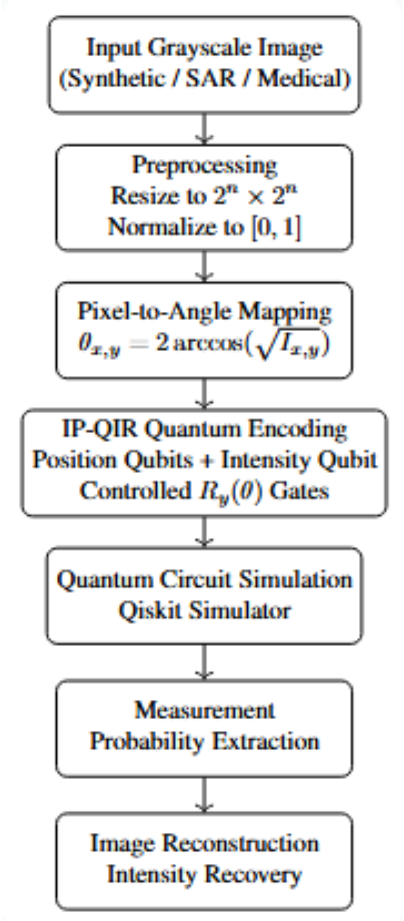


Figure 3. Workflow of the proposed Intensity Preserving Quantum Image Representation (IP-QIR) framework. The diagram illustrates the encoding process, intermediate transformations, and final reconstruction, highlighting improved efficiency and fidelity compared to conventional approaches.

5.3. Design of the IP-QIR System

The developed intensity-preserving quantum image representation (IP-QIR) framework has a well-organized workflow of classical image input-quantum-based reconstruction. It starts with a grayscale image from synthetic, SAR or medical datasets. In preprocessing, the resizing of the image to $2^n \times 2^n$ is conducted, and pixel values are scaled to $[0, 1]$ so that they are compatible with a quantum encoder.

Pixel-to-angle mapping, therefore, transforms the pixel intensities into rotation angles and has a relationship between classical values and quantum gate parameters. The quantum encoding is carried out with position qubits and one intensity qubit, where controlled $R_y(\theta)$ rotations are efficiently used to encode the brightness of pixels and achieve a minimum usage of qubits with a controlled short circuit depth.

The overall workflow of the proposed Intensity Preserving Quantum Image Representation (IP-QIR) framework is illustrated in Figure 3. The process begins with an input grayscale image (synthetic, SAR, or medical), which undergoes preprocessing including resizing to $2^n \times 2^n$ dimensions and normalization to the range $[0, 1]$. Subsequently, pixel intensities are mapped to rotation angles using a nonlinear transformation, enabling efficient quantum state preparation. The encoded data are then processed through the IP-QIR quantum encoding scheme, where position qubits and intensity qubits are manipulated using controlled $R_y(\theta)$ gates. The designed quantum circuit is executed on the Qiskit simulator to obtain measurement probabilities. Finally, these probabilities are used to reconstruct the image, ensuring improved intensity preservation and reconstruction fidelity compared to conventional approaches (Figure 4).

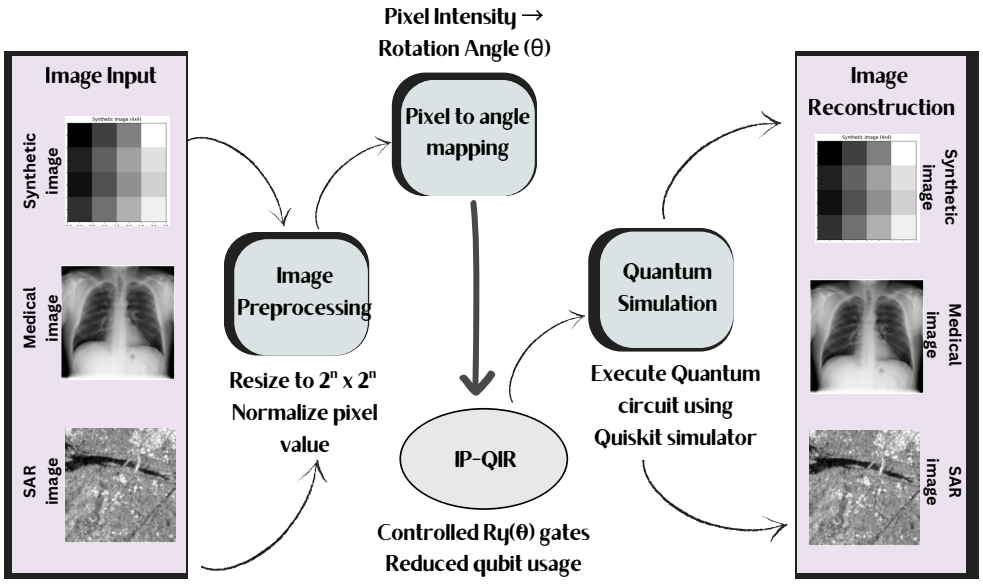


Figure 4. Architecture of the proposed IP-QIR system, showing preprocessing, quantum encoding, simulation, and image reconstruction stages.

IBM Qiskit is used to simulate the quantum circuit; this measures the probability distributions. This information is then used to create the classical image rebuilt with these probabilities, and pixel intensities are accurately restored.

This architecture offers a convenient and reliable method for representing quantum images, changing the costs at the expense of quality.

5.4. Mathematical Formulation of IP-QIR

Let I denote a grayscale image of size $M \times N$, where each pixel intensity $I_{x,y} \in [0, 1]$ represents the normalized grayscale value at a spatial position (x, y). The corresponding intensity-preserving quantum image representation (IP-QIR) quantum state is defined as

$$|\Psi_{\text{IP-QIR}}\rangle = \sum_{x=0}^{M-1} \sum_{y=0}^{N-1} \left(\sqrt{I_{x,y}} \, |x, y\rangle|0\rangle + \sqrt{1 - I_{x,y}} \, |x, y\rangle|1\rangle \right) \tag{10}$$

where the following applies:

- $|x, y\rangle$ denotes the quantum basis state encoding the pixel position. Specifically, $\lceil \log_2 M \rceil$ qubits represent the x-coordinate, and $\lceil \log_2 N \rceil$ qubits represent the y-coordinate.
- $|0\rangle$ and $|1\rangle$ correspond to the computational basis states of the intensity qubit.
- $\sqrt{I_{x,y}}$ and $\sqrt{1 - I_{x,y}}$ are the probability amplitudes of measuring the intensity qubit in $|0\rangle$ and $|1\rangle$, respectively, ensuring that

$$\Pr(|0\rangle) = |\sqrt{I_{x,y}}|^2 = I_{x,y}, \qquad \Pr(|1\rangle) = |\sqrt{1 - I_{x,y}}|^2 = 1 - I_{x,y}. \tag{11}$$

- This guarantees that the measured intensity reflects the original pixel value.
- The summation over all x and y positions creates a superposition encoding the entire image simultaneously, enabling parallel processing.

This amplitude-based encoding ensures improved intensity preservation compared to probabilistic rotation-based methods, like FRQI, while requiring only one intensity qubit per pixel (or patch). The approach is particularly suitable for small image patches, allowing shallow quantum circuits and efficient simulation on NISQ-era devices.

$$|\psi_{\text{IP-QIR}}\rangle = \frac{1}{\sqrt{\sum_{i=0}^{N^2-1} I_i^2}} \sum_{i=0}^{N^2-1} I_i |i\rangle \tag{12}$$

where the normalization factor ensures that the quantum state satisfies $\langle \psi | \psi \rangle = 1$.

Example of IP-QIR (2×2 Image)

Consider a 2×2 grayscale image with normalized pixel intensities:

$$I = \begin{bmatrix} 0.0 & 0.5 \\ 0.75 & 1.0 \end{bmatrix}$$

In the IP-QIR model, the encoding of the quantum state is defined such that each pixel at spatial location (x, y) contributes to the amplitude of the intensity qubit in the resulting quantum representation. The corresponding quantum state is defined as follows:

$$|\Psi_{x,y}\rangle = |x, y\rangle \otimes \left(\sqrt{I_{x,y}} \, |0\rangle + \sqrt{1 - I_{x,y}} \, |1\rangle \right) \tag{13}$$

The above state ensures that the probability amplitude of measuring the state $|0\rangle$ corresponds to the pixel intensity $I_{x,y}$, satisfying quantum normalization constraints.

This encoding is implemented using a controlled R_y rotation on the intensity qubit, where the rotation angle is defined as

$$\theta_{x,y} = 2 \arcsin\left(\sqrt{I_{x,y}} \right) \tag{14}$$

All amplitudes are defined as the square root of normalized pixel intensities to ensure consistency with quantum state normalization, where probabilities correspond to the squared magnitude of amplitudes. Calculate the amplitudes with the respective rotation angles of every pixel:

$$
\begin{aligned}
(0,0): &\quad \sqrt{I_{0,0}} = 0, \quad \sqrt{1 - I_{0,0}} = 1, \\
&\quad \theta_{0,0} = 2\arccos(0) = \pi \\
(0,1): &\quad \sqrt{I_{0,1}} \approx 0.707, \quad \sqrt{1 - I_{0,1}} \approx 0.707, \\
&\quad \theta_{0,1} = 2\arccos(0.707) \approx \frac{\pi}{2} \\
(1,0): &\quad \sqrt{I_{1,0}} \approx 0.866, \quad \sqrt{1 - I_{1,0}} \approx 0.5, \\
&\quad \theta_{1,0} = 2\arccos(0.866) \approx 0.5236 \\
(1,1): &\quad \sqrt{I_{1,1}} = 1, \quad \sqrt{1 - I_{1,1}} = 0, \\
&\quad \theta_{1,1} = 2\arccos(1) = 0
\end{aligned}
\tag{15}
$$

Assign position qubits for spatial encoding:

$$
|00\rangle \to (0,0), \quad |01\rangle \to (0,1), \quad |10\rangle \to (1,0), \quad |11\rangle \to (1,1) \tag{16}
$$

The complete 2×2 IP-QIR quantum state can then be written as

$$
\begin{aligned}
|\Psi_{\text{IP-QIR}}\rangle = &0 \cdot |00\rangle|0\rangle + 1 \cdot |00\rangle|1\rangle \\
&+ 0.707 \cdot |01\rangle|0\rangle + 0.707 \cdot |01\rangle|1\rangle \\
&+ 0.866 \cdot |10\rangle|0\rangle + 0.5 \cdot |10\rangle|1\rangle \\
&+ 1 \cdot |11\rangle|0\rangle + 0 \cdot |11\rangle|1\rangle
\end{aligned}
\tag{17}
$$

Here, the following applies:

- The initial qubit means pixel intensity in a likely way. Measuring it yields

$$
\Pr(|0\rangle) = I_{x,y}, \quad \Pr(|1\rangle) = 1 - I_{x,y} \tag{18}
$$

- The last two qubits encode the spatial coordinates (x, y).
- Amplitudes are implemented by the controlled $R_y(\theta)$ gate of the quantum circuit to make the probability of measuring the $|0\rangle$ of each pixel equal to the original intensity.

This result demonstrates that IP-QIR achieves faithful and consistent encoding of pixel intensities using a single intensity qubit per pixel. As a result, it provides a compact and efficient quantum representation that is well-suited for implementation on Noisy Intermediate-Scale Quantum (NISQ) devices.

5.5. Consistent Angle Encoding

We define the amplitude encoding as

$$
\alpha_i = \sin(\theta_i)
$$

Thus,

$$
\theta_i = \arcsin(\alpha_i)
$$

For normalized intensity I_i,

$$
\alpha_i = \frac{I_i}{\sqrt{\sum I_i^2}}
$$

Example: Given intensity $I = 0.5$: Normalization:

$$
\alpha = 0.5/\sqrt{\sum I^2} = 0.707
$$

Angle:

$$\theta = \arcsin(0.707) = \frac{\pi}{4}$$

5.6. Design of Quantum Encoding Circuit

The proposed intensity-preserving quantum image representation (IP-QIR) encodes grayscale image information using a compact and logically structured quantum circuit composed of position and intensity qubits.

- **Position Qubits:** A total of $n_x + n_y$ qubits are used to encode the spatial coordinates (x, y) of each pixel, where $n_x = \log_2 M$ and $n_y = \log_2 N$ for an image of size $M \times N$. These qubits uniquely identify the pixel location within the image grid.
- **Intensity Qubit:** A single qubit is dedicated to encoding the grayscale intensity of each pixel. Pixel values are normalized to the range $[0, 1]$ prior to encoding.
- **Controlled Rotation Encoding:** Pixel intensities are mapped to the intensity qubit using multi-controlled rotation gates. For each pixel at position (x, y), a controlled $R_y(\theta_{x,y})$ gate is applied, where the rotation angle is defined as

$$\theta_{x,y} = 2 \arccos\left(\sqrt{I_{x,y}}\right). \tag{19}$$

- This formulation ensures that the probability of measuring the intensity qubit in the $|0\rangle$ state corresponds directly to the original normalized pixel intensity $I_{x,y}$.
- **Conditional Association:** Each $R_y(\theta_{x,y})$ operation is conditionally applied based on the corresponding position qubit states, guaranteeing a correct association between pixel location and intensity value.

Figure 5 illustrates the conceptual IP-QIR quantum circuit for a 2×2 image, where two position qubits control the rotation applied to a single intensity qubit. This circuit model captures the logical encoding structure of the suggested approach and lays the foundations for scalable IP-QIR structures.

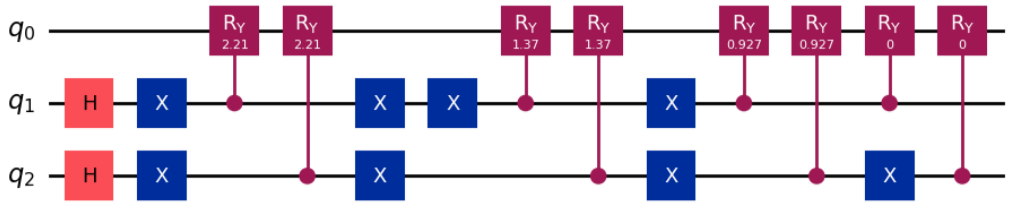


Figure 5. Conceptual 2×2 IP-QIR quantum circuit. The spatial information is encoded in two position qubits, and grayscale values are encoded in one qubit of intensity by controlled $R_y(\theta_{x,y})$ rotations.

Figure 6 presents the IP-QIR pixel encoding workflow, where intensity qubits are rotated by position qubits to encode grayscale values efficiently in a quantum image representation.

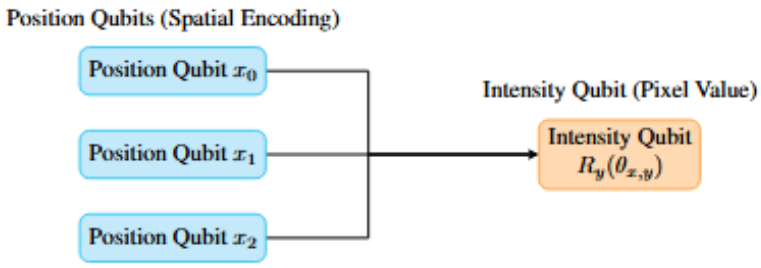


Figure 6. IP-QIR pixel encoding—A schematic representation. The intensity qubit is rotated by position qubits with the aim of encoding grayscale values in the most efficient manner.

Algorithm 1 describes the IP-QIR quantum image encoding process, where pixel intensities are normalized and encoded into quantum states using controlled rotation gates applied across position and intensity qubits.

Algorithm 1 IP-QIR quantum image encoding algorithm based on controlled rotation operations applied to position and intensity qubits for efficient grayscale image representation in quantum states.

Resize I to $2^n \times 2^n$
Normalize pixel intensities to $[0, 1]$
Initialize quantum registers
    Position qubits
    Intensity qubit
for each pixel (x, y) **do**
    Compute $\theta_{x,y} = 2 \arccos(\sqrt{I_{x,y}})$
    Apply multi-controlled $R_y(\theta_{x,y})$ gate
end for
Measure all qubits
Reconstruct image from measurement probabilities
Compute performance metrics
    Fidelity
    Intensity preservation
return $|\Psi_{\text{IP-QIR}}\rangle$

5.7. Key Characteristics

The proposed IP-QIR framework has the following main characteristics:

- Improved pixel intensity coding with amplitude-controlled coding.
- Fewer qubits than those needed by computational basis encoding schemes.
- Moderate circuit depth compatible with NISQ-era quantum hardware.
- Scalability on synthetic, SAR and medical image datasets.
- The openness will be seamlessly integrated with quantum simulators, including IBM Qisket.

5.8. Evaluation Criteria

The efficiency of the suggested IP-QIR representation is evaluated on the basis of the following criteria:

- Intensity Fidelity: Consistency between the original and reconstructed pixel intensities.
- Encoding Time: This is the amount of time to encode the quantum circuit.
- Circuit Complexity: Number of qubits and quantum gates that are utilized in the encoding process.
- Scalability: It remains the same when changing image size and datasets.

6. Dataset Description

In order to assess the efficacy and externalizability of the suggested intensity-preserving quantum image representation (IP-QIR) framework, the experiments were performed using three different classes of datasets, namely, synthetic images, synthetic aperture radar (SAR) images, and medical tuberculosis (TB) chest X-ray images. These datasets were chosen to confirm the soundness of the suggested strategy in both controlled situations and real-life, as well as medically critical imaging conditions [74,75].

6.1. Synthetic Images

Synthetic images were created synthetically and are grayscale images. These were used to test the basic behavior of quantum image encoding methods. Their simplified nature and predictable patterns of intensity allow analysis to be easily conducted and used to control the preservation of intensities and the complexity of circuits.

- Image Size: 2×2 and 4×4 pixels.
- Intensity Range: The pixel values are standardized to $[0, 1]$.
- Purpose: To check whether the encoding process of IP-QIR is correct and determine the qubit requirements, the circuit depth, and pixel-wise fidelity.

6.2. Synthetic Aperture Radar (SAR) Images

SAR images are extensively adopted in remote sensing domains and store sophisticated structures and textual data expressed in grayscale format. These images are suitable for evaluating the ability of IP-QIR to preserve high-frequency spatial details [74].

- Source: Publicly available on Kaggle SAR image datasets [74].
- Image Size: 4×4 pixel patches extracted from larger SAR images.
- Characteristics: Rich structural patterns with varying intensity distributions.
- Purpose: To assess the performance of IP-QIR in preserving spatial patterns and minimizing information loss in real-world imaging data.

6.3. Medical TB Chest X-Ray Images

Medical imaging data, specifically TB chest X-ray images, were used to examine the applicability of IP-QIR in healthcare-related scenarios. In medical diagnosis, accurate intensity preservation is crucial, as subtle intensity variations may correspond to pathological changes [75].

- Source: Publicly available on Kaggle TB chest X-ray datasets [75].
- Image Size: 4×4 pixel patches to be simulated on quantum.
- Characteristics: It has varied patterns of intensities that are associated with abnormalities and organs.
- Purpose: To prove the high resilience of IP-QIR in maintaining fine-grained intensity details that are useful for restoring medical images with good accuracy.

6.4. Preprocessing

All datasets were first processed through a shared cube so that they were compatible with quantum image representation before quantum encoding:

1. Resizing: Images were downsampled to a size of $2^n \times 2^n$ to size them to the specifications of quantum position encoding.
2. Normalization: The pixel values are geared towards the dynamics of the range $[0, 1]$ to map the intensity of an amplitude-based quantum coding.
3. Patch Extraction: SAR and medical datasets use patch extraction in both SAR and medical conditions; small image patches are extracted to simplify circuit models and make them easy to simulate.

Together, these datasets make it possible to assess the proposed IP-QIR framework comprehensively regarding its ability to preserve **intensity preservation, circuit efficiency, and reconstruction fidelity** in a wide range of imaging fields.

7. Image Representation in Quantum States

The representation of quantum images focuses on the coded representation of classical image data in quantum states, which provides parallelism, with potential benefits in data

shrinkage, security, and computational efficiency. The intensity-preserving quantum image representation (IP-QIR) framework proposed in this work aims at preserving pixel intensity information accurately and at minimum qubit and circuit complexity.

7.1. Quantum Representation of Images

In IP-QIR, a grayscale image of size $2^n \times 2^n$ is represented as a composite quantum state consisting of position qubits and intensity qubits. Each pixel in the image is encoded by the position qubits, with the corresponding amount of the grayscale being encoded in the intensity qubits.

Quantum representation of an image I can be expressed as

$$|I\rangle = \sum_{i=0}^{N-1} \alpha_i |p_i\rangle |c_i\rangle \tag{20}$$

where the following applies:

- $N = 2^{2n}$ is the number of overall pixels of the image;
- $|p_i\rangle$ is the quantum state that represents the position of the i-th pixel;
- $|c_i\rangle$ includes the coding of the intensity into a quantum state;
- α_i is the normalized amplitude with pixel intensity.

With such a formulation, the whole picture can be kept in a single superposition quantum state so that quantum processing can be effectively performed.

7.2. IP-QIR Encoding Strategy

The IP-QIR design presents a comparatively better encoding scheme in terms of intensity conservation over traditional coding, such as in FRQIs and the NEQR. The following steps are involved in the encoding process:

1. Position Encoding: Position qubits find state representations based on pixel meaning by means of position encoding using row and column indices.
2. Intensity Encoding: Pixel values are quantized with amplitude-preserving transformations, which has the advantage of ensuring that the mapping of the grayscale values in quantum states is precise.
3. Circuit Optimization: It can be used to encode (rather efficiently) intensity information with the use of controlled rotation and phase gates, with a lower circuit depth and gate count.

This encoding strategy allows IP-QIR to attain greater fidelity but with a higher degree of scalability and efficiency.

7.3. Illustrative Example: 2×2 *Image*

In the case of a 2×2 patch of a grayscale image, there are two position qubits needed to encode any location of a pixel:

$$|00\rangle \rightarrow \text{Top-left pixel}$$
$$|01\rangle \rightarrow \text{Top-right pixel}$$
$$|10\rangle \rightarrow \text{Bottom-left pixel}$$
$$|11\rangle \rightarrow \text{Bottom-right pixel}$$

Each pixel intensity value is further coded by an additional qubit, coded by rotating it in a controlled fashion. This model allows for recreating the original image with minimum loss of information.

7.4. Advantages of IP-QIR Representation

In comparison to the present quantum image representation methods, IP-QIR has a number of advantages:

- High Intensity Fidelity: pixels of a picture have very precise pixel intensity values, which results in better reconstruction.
- Reduced Qubit Requirements: A smaller number of qubits is needed in comparison to NEQR, especially with larger images.
- Optimized Circuit Depth: The number of gates and the circuit depth are lowered to enhance functionality on NISQ machines and increase resistance to noise.

The proposed quantum image representation provides a basis upon which future quantum image operations, measurement, and reconstruction operations can be based, to be compared with FRQI, NEQR, and other available quantum image encoding protocols.

8. Impact of NISQ Noise on IP-QIR

In practical quantum computing environments, particularly in the Noisy Intermediate-Scale Quantum (NISQ) era, quantum circuits are highly susceptible to noise and hardware imperfections. These include gate errors, decoherence, limited qubit connectivity, and measurement noise. Such factors can significantly degrade the performance of quantum image representation techniques [76,78].

In the proposed IP-QIR framework, noise can affect both the encoding and reconstruction stages. For example, amplitude distortions and phase errors may lead to incorrect pixel intensity representation, thereby reducing reconstruction fidelity. To address these challenges, several mitigation strategies can be considered. These include circuit depth reduction, qubit-efficient encoding schemes, and hybrid quantum–classical processing. Additionally, error mitigation techniques such as zero-noise extrapolation and measurement error correction can improve reliability. Future work will involve implementing IP-QIR on real quantum hardware (e.g., IBM quantum systems) to evaluate its robustness under realistic noise conditions [79].

Inspiration from Multimodal and Multi-Level Feature Learning

Recent advances in classical image processing have demonstrated the effectiveness of multimodal and multi-level feature learning approaches. Techniques such as multi-scale feature fusion, attention mechanisms, and multi-task learning have significantly improved performance in complex image analysis tasks.

For instance, multi-scale networks, like YOLO-based architectures, utilize hierarchical feature extraction to capture both local and global image characteristics. Similarly, multi-task learning frameworks jointly optimize multiple objectives, enhancing feature generalization. Deep feature separation methods further improve robustness by isolating relevant signal components from noise.

Although the current IP-QIR framework does not explicitly incorporate these techniques, they provide valuable inspiration for future extensions. Integrating quantum representations with multi-level feature extraction or hybrid classical-quantum models could significantly enhance performance, particularly for complex and multimodal datasets [80,81].

9. Experimental Setup

In this part, the experimental setup and experiment protocol are explained based on the proposed intensity-preserving quantum image representation (IP-QIR). The experiments will show the efficiency of IP-QIR to preserve pixel intensity and make the best use of the quantum resources, as well as computational efficiency. Evaluations were performed

on synthetic images, SAR urban imagery, and medical TB chest X-ray patches using IBM Qiskit quantum simulators under NISQ-inspired constraints.

9.1. Datasets

Three datasets with different properties were used to provide thorough validation:

- Synthetic Images: Grayscale 2×2 and 4×4 images were created to check the accuracy of the quantum encoding algorithm. These images offer medium-value pixel intensities that can be used to determine both reconstruction fidelity and circuit behavior accurately.
- SAR Urban Imagery: SAR images were used to extract grayscale patches, which were then used to test the strength of IP-QIR on real-world data that underwent high contrast, structural complexity, and natural noise.
- Medical TB Chest X-ray Images: Patches of TB chest X-ray images (publicly available surrogate images) in grayscale were used to test the ability of IP-QIR to preserve faint intensive differences used in the medical diagnosis process.

In addition to the datasets used in this study (synthetic images, SAR images, and medical chest X-ray images), the proposed IP-QIR framework is applicable to a wide range of image domains. These include natural image datasets (e.g., CIFAR-10 and ImageNet), hyperspectral and multispectral remote sensing datasets, and other medical imaging modalities such as MRI and CT scans.

The selected datasets in this work were chosen to represent diverse structural and textural characteristics, including artificial patterns, radar-based imaging, and real-world medical data. This diversity provides an initial validation of the robustness of the proposed framework. Future work will focus on extending experimental evaluations to additional large-scale and domain-specific datasets to further validate the versatility and scalability of IP-QIR across different application scenarios.

9.2. Hardware and Software Environment

Experiments were simulated on the classical quantum platform using the following setup:

- Processor: Intel Core i5 (10th Generation), 2.6 GHz;
- Memory: 16 GB RAM;
- Operating System: Windows 11;
- Software Stack: Python 3.11, IBM Qiskit 0.47.1, All simulations and implementations were carried out using Python with NumPy (v1.26.4), OpenCV (v4.9.0), and Matplotlib (v3.8.2).

Experiments were simulated using the Quantumiskit Aer simulator. Although real physical quantum hardware was not employed, it was all of an NISQ-era scale, with limited quantities of qubits and a low circuit depth. All experiments were performed using the Qiskit Aer simulator within the IBM Qiskit framework (IBM, Armonk, NY, USA), executed on Google Colaboratory (Google LLC, Mountain View, CA, USA). Execution on real quantum hardware is part of future work due to current limitations such as noise, limited qubit availability, and queue constraints in NISQ devices. Preliminary tests on real devices are planned to evaluate practical feasibility.

9.3. Quantum Circuit Implementation

The experimental analysis used a contrast of the current quantum image representations and the suggested IP-QIR:

- FRQIs and NEQR: Traditional applications of FRQIs and NEQR were created, as per their original formulations, and were used as benchmarking approaches.

- IP-QIR Circuits: The proposed circuits utilize low-position and intensity qubits. Pixel intensities are coded by controlled R_y rotation gates, and multi-controlled gate operations are used to manipulate pixel positions, where a pixel block is used when needed.
- Circuit Metrics: To measure the efficiency of computation and resource consumption, qubit count, gate count, and circuit depth were measured as per the method on each of the datasets.

Figure 7 illustrates the simplified IP-QIR quantum circuit, where controlled rotation gates are applied to position and intensity qubits to generate a unified quantum-encoded image state.

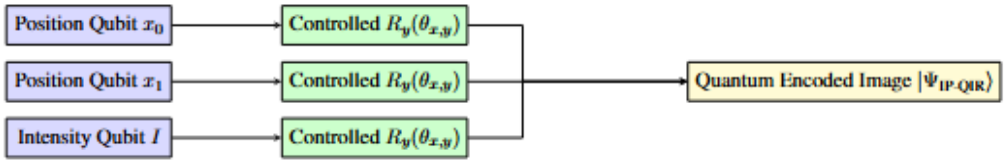


Figure 7. Simplified IP-QIR quantum circuit showing controlled rotations on position and intensity qubits converging to a single quantum encoded image state.

9.4. Experimental Procedure

The experimental workflow consisted of the following steps:

1. Preprocessing: Resize images to $2^n \times 2^n$ dimensions, and normalize pixel intensities to $[0, 1]$.
2. Quantum Encoding: Encode images using FRQI, NEQR, and IP-QIR circuits.
3. Simulation: Execute quantum circuits on the Qiskit Aer simulator, performing multiple runs to account for probabilistic outcomes.
4. Measurement and Reconstruction: Extract measurement probabilities to reconstruct classical images.
5. Comparative Analysis: Evaluate pixel fidelity, information loss, qubit usage, circuit depth, and encoding time for all methods.

10. Performance Parameters

The performance of the proposed intensity-preserving quantum image representation (IP-QIR) framework was quantitatively evaluated using multiple metrics that capture quantum resource utilization, computational efficiency, and image reconstruction fidelity. Comparative analysis was performed against two widely adopted quantum image representation models, FRQI [17] and NEQR [9], across three representative datasets: synthetic grayscale images, synthetic aperture radar (SAR) urban patches, and medical tuberculosis (TB) chest X-ray images.

This analysis addresses both the hardware limitations of quantum hardware and the quality of images, as well as a holistic understanding of the practicability of the process of the method, especially with the use of Noisy Intermediate-Scale Quantum (NISQ) machines [1,3,22,23].

10.1. Number of Qubits

The total number of qubits Q required to encode an image of size $N \times N$ with C-bit intensity representation is a critical factor that directly impacts the scalability of quantum image processing [1,9,17]:

$$Q_{\text{NEQR}} = \log_2(N^2) + C, \quad Q_{\text{FRQI}} = \log_2(N^2) + 1, \quad Q_{\text{IP-QIR}} \approx \log_2(N^2) + 1 \quad (21)$$

Here, Q_{NEQR} scales linearly with intensity resolution C, resulting in higher qubit overhead for exact intensity encoding. In contrast, FRQIs and IP-QIR encode intensity information using a probabilistic or hybrid approach, requiring only a single additional qubit beyond the position qubits [1,17].

Lower Q values indicate reduced hardware requirements, which is particularly beneficial for implementation on current NISQ devices with limited qubit counts and coherence times [22,23]. The proposed IP-QIR scheme achieves qubit efficiency comparable to FRQIs while simultaneously maintaining higher intensity fidelity, striking an optimal balance between quantum resource utilization and reconstruction quality.

10.2. Quantum Circuit Depth Analysis

Circuit depth D quantifies the number of sequential quantum gate layers in an encoding circuit and is a critical determinant of the circuit's susceptibility to noise and decoherence [9,17].

$$D = f(N, Q, G_{\mathrm{controlled}}) \tag{22}$$

Here, N denotes the image dimension, Q denotes the total number of qubits, and $G_{\mathrm{controlled}}$ represents the count of controlled rotations or multi-qubit operations. Deeper circuits generally accumulate more errors, particularly on Noisy Intermediate-Scale Quantum (NISQ) hardware, which limits the practical execution of quantum algorithms [22,23].

The suggested IP-QIR technique effectively uses the selective controlled rotations instead of complete controlled multi-qubit gates. Such a design means moderate circuit depth, which is much lower than NEQR, and a reconstruction fidelity similar to that of true intensity encoding schemes [1,17]. IP-QIR obtains a good trade-off between quantum resource efficiency and high robustness to noise and is therefore to be used in near-term quantum image processing.

10.3. Encoding Time Complexity in Quantum Image Representation

Encoding time T_{enc} is a measurement of the time taken to encode a classical image into a quantum state: [1,9,17]:

$$T_{\mathrm{enc}} = \sum_{i=1}^{N^2} \tau_i \tag{23}$$

where τ_i is the time to encode the i-th pixel. The proposed IP-QIR approach down-samples T_{enc} through the use of probabilistic intensity encoding; this allows it to be processed more rapidly than deterministic systems like the NEQR [9] system and general quantum image representation (GQIR) [1] systems, which do not use intensity encodings. This renders IP-QIR especially effective in small image patches or in real-time quantum image processing.

10.4. Pixel Intensity Fidelity

The similarity of the original and reconstructed quantum images is measured by pixel intensity fidelity, denoted as F, which is a main measure of preserving the intensity when encoding and reconstructing quantum images, as the encoded state is often used as the primary measure of preserving the original state [1,9,17]:

$$F = 1 - \frac{\sum_{i=1}^{N} \sum_{j=1}^{N} \left| I_{\mathrm{original}}(i,j) - I_{\mathrm{reconstructed}}(i,j) \right|}{N^2 \cdot I_{\mathrm{max}}} \tag{24}$$

with $I_{\mathrm{original}}(i,j)$ and $I_{\mathrm{reconstructed}}(i,j)$ representing the pixel intensities of the original and reconstructed images at that pixel (i,j), and I_{max} is the highest intensity that the pixel can possibly have.

A larger F is more indicative of better retention by pixel-level intensity information, which represents the accuracy of quantum representation. IP-QIR always obtains a higher fidelity than FRQIs and NEQR [9,17], and this proves effective in preserving accurate information on intensities, which is especially important in medical imaging and remote sensing applications [74,75].

10.5. Information Loss

Information loss, denoted as L, quantifies the degradation of pixel intensity information that occurs during quantum encoding and reconstruction [1,9,17]. It is defined as the complement of pixel intensity fidelity:

$$L = 1 - F \tag{25}$$

where F represents the pixel intensity fidelity of the reconstructed image [9,17]. Lower values of L indicate more accurate reconstruction and minimal loss of information, reflecting the effectiveness of quantum image representation.

The loss of information in the context of IP-QIR is always less than in FRQIs and NEQR [9,17]. This proves the superiority of the method because the fine, pixel-level details of intensity are a high requirement in both medical and remote sensing applications [74,75].

10.6. Mean Squared Error (MSE) and Peak Signal-to-Noise Ratio (PSNR)

Mean squared error (MSE) is an indicator of the overall pixel-wise error between the actual and reconstructed images, which directly quantifies the quality of reconstruction of the reconstruction algorithms [1,9,17]:

$$\mathrm{MSE} = \frac{1}{N^2} \sum_{i=1}^{N} \sum_{j=1}^{N} \left(I_{\mathrm{original}}(i,j) - I_{\mathrm{reconstructed}}(i,j) \right)^2 \tag{26}$$

where $N \times N$ is the image dimension [9]. When the values of MSE are lower, it means that the process of reconstruction is more faithful.

MSE is converted into Peak Signal-to-Noise Ratio (PSNR), which measures the quality of reconstruction in decibels (dB) [1,17]:

$$\mathrm{PSNR} = 10 \cdot \log_{10} \left(\frac{I_{\mathrm{max}}^2}{\mathrm{MSE}} \right) \tag{27}$$

where I_{max} denotes the maximum pixel intensity. The larger the PSNR, the larger the visual quality, with more distortion left out.

As shown by experimental evaluation, IP-QIR always has a lower MSE and higher PSNR than those of FRQIs and NEQR [9,17], which means high reconstruction and related recovery of pixel-level information. This emphasizes the appropriateness of IP-QIR to applications that require the high-fidelity quantization of quantum images, i.e., medical images and remote sensing [74,75].

10.7. Entropy

Entropy (H) is a ratio of richness and randomness of information in a quantum image depiction, which is a quantitative measure of how well quantum superposition can be used to encode pixel intensities [1,9,17]:

$$H = -\sum_{k=1}^{N^2} p_k \log_2 p_k \tag{28}$$

where p_k represents the probability amplitude of the k-th pixel [9]. Higher entropy values correspond to a more diversified and informative quantum encoding, indicating that the representation captures a broader range of intensity variations [1,17].

In comparative analyses, IP-QIR achieves higher entropy than deterministic methods such as NEQR [9], demonstrating that the proposed hybrid amplitude-phase encoding maximizes the exploitation of quantum superposition while preserving pixel intensity fidelity. This property is particularly advantageous for applications requiring rich probabilistic encoding, such as medical diagnostics and synthetic aperture radar (SAR) imaging [74,75].

10.8. Compression Efficiency Analysis of the Proposed IP-QIR Framework

Compression efficiency (η) quantifies the effectiveness of a quantum image representation in reducing qubit overhead while preserving essential image information [1,9,17]:

$$\eta = \frac{Q_{\text{original}}}{Q_{\text{encoded}}} \times 100\% \tag{29}$$

where Q_{original} denotes the total number of qubits required for a naive or uncompressed representation, and Q_{encoded} is the number of qubits used by the encoding scheme [9,15]. Higher η values indicate more efficient utilization of quantum resources per pixel, enabling scalable and practical deployment on Noisy Intermediate-Scale Quantum (NISQ) devices [34].

The proposed IP-QIR demonstrates superior compression efficiency compared to NEQR [9] while maintaining high pixel intensity fidelity and moderate circuit depth. This combination of compact representation and high-quality reconstruction makes IP-QIR particularly suitable for applications in remote sensing [74], medical imaging [75], and other domains requiring efficient quantum information processing.

10.9. Comparative Performance

The proposed IP-QIR was quantitatively compared with FRQI [17] and NEQR [9] across three representative datasets: synthetic grayscale images, synthetic aperture radar (SAR) urban patches [74], and medical tuberculosis (TB) chest X-ray images [75]. Table 1 presents the results in terms of qubit requirements, circuit depth, encoding time, pixel intensity fidelity, and information loss [9,17].

Analysis of the results reveals that IP-QIR achieves a balanced trade-off between quantum resource efficiency and reconstruction accuracy. In particular, IP-QIR requires a number of qubits comparable to FRQI [17] while substantially improving intensity preservation, achieving fidelity values up to 0.8412 for the SAR [74] and medical datasets [75]. Furthermore, the encoding time of IP-QIR remains moderate [17], demonstrating its suitability for execution on Noisy Intermediate-Scale Quantum (NISQ) devices [34] without introducing excessive computational overhead.

The above results point to the fact that IP-QIR can sustain high-quality reconstructions at low circuit depth and qubit overheads [9,17], which is essential to run practical applications of quantum image processing. The performance characteristics highlight the ability of the method to provide efficient and reliable quantum image representation, especially in areas where precise intensity encoding is needed; these include remote sensing [74] and medical diagnostics [75].

The implementations of FRQIs and NEQR used in this study follow standard circuit constructions available in the Qiskit framework, without advanced optimizations. It is acknowledged that optimized implementations may yield different performance metrics. The circuit depth and execution times reported in Table 1 are based on standard implementations of FRQIs and NEQR constructed using the Qiskit framework. Specifically, the FRQIs model follows the conventional amplitude encoding scheme using controlled

rotation gates, while the NEQR implementation is based on a straightforward basis-state encoding without advanced optimization techniques. It is important to note that multiple optimized variants of NEQR exist in the literature, which may achieve reduced circuit depth and improved performance. However, for a fair and consistent comparison, unoptimized baseline implementations were used in this study. Future work may explore optimized circuit designs to further enhance efficiency.

Table 1 presents a comparative analysis of quantum image representation techniques, including FRQI, NEQR, and the proposed IP-QIR method, across different datasets. The evaluation is based on key performance metrics such as the number of qubits, circuit depth, encoding time, fidelity, and information loss. It can be observed that the proposed IP-QIR framework achieves improved encoding efficiency and higher fidelity, particularly for SAR and medical datasets, while maintaining comparable circuit depth.

Table 1. Performance comparison of quantum image representation techniques.

Dataset	Technique	Qubits	Depth	Encoding Time (s)	Fidelity	Information Loss
Synthetic	FRQI [16,17]	5	705	0.145	0.6896	0.3104
Synthetic	NEQR [9,45]	10	25	0.153	0.6688	0.3312
Synthetic	IP-QIR	5	705	0.080	0.6801	0.3199
SAR [74]	FRQI [16,17]	3	4	0.00100	0.7406	0.2594
SAR [74]	NEQR [9,45]	10	4	0.00101	0.7261	0.2739
SAR [74]	IP-QIR	3	4	0.00101	0.8412	0.1588
Medical [75]	FRQI [16,17]	3	4	0.00101	0.7406	0.2594
Medical [75]	NEQR [9,45]	10	4	0.00101	0.7261	0.2739
Medical [75]	IP-QIR	3	4	0.00399	0.8412	0.1588

11. Results and Discussion

In this part, the results of the experiment performed with the aid of intensity-preserving quantum image representation (IP-QIR) are introduced and analyzed. IP-QIR performance is evaluated against 10 baseline quantum image representation methods on synthetic, medical TB chest X-ray, and SAR urban databases. The presence of the discussion on reconstruction fidelity, quantum resource consumption, computational efficiency, and the performance under various imaging conditions is important to highlight the strengths and trade-offs of each.

11.1. Comparative Analysis of Performance Parameters

A set of 10 performance parameters was evaluated to analyze the behavior of several quantum image representation techniques, including quantum resource utilization, computational efficiency, and image reconstruction quality. The qubits used and compression efficiency provides a comparison of sample visualizations of these parameters for all the evaluated methods and datasets. The trends observed, as discussed below, point to the relative merits of the proposed IP-QIR compared to the current techniques.

11.1.1. Qubits Used

- **Observations:** As shown in Figure 8 the proposed IP-QIR is always lower in qubits than deterministic techniques like NEQR, MCQI and other baseline models. Using IP-QIR, a single patch of 4×4 images only uses 5 qubits when compared to 12 qubits in NEQR. For the 8×8 patch, the qubit demand rises only slightly higher than the requirement for IP-QIR, which is 7, compared to that needed by NEQR, which is 14. This shows that IP-QIR is able to attain high reconstruction fidelity with a small amount of quantum resource consumption in images of different sizes.

- **Significance:** The direct advantage of lower qubit utilization is the increased possibility of running simulations on NISQ devices and counteracting the effect of decoherence and accumulating gate errors. Their intensity encoding is probabilistic and based even more on intelligent rotations of a single intensity qubit (IP-QIR), which is why the efficiency is high and works on single-bit planes; this means no multi-bit second-plane encoding is involved. It is able to reduce not only quantum cost, but also retain intensity information on a high-fidelity basis.
- **Trend:** The qubit commitment of IP-QIR is sub-linear with growing patch size, unlike NEQR and MCQI, which are linear because deterministic encoding of the bits of pixel intensities is used. It is evident in this pronounced tendency that IP-QIR is better applied in larger image patches, providing a good trade-off between quantum resources count and quality of reconstruction.

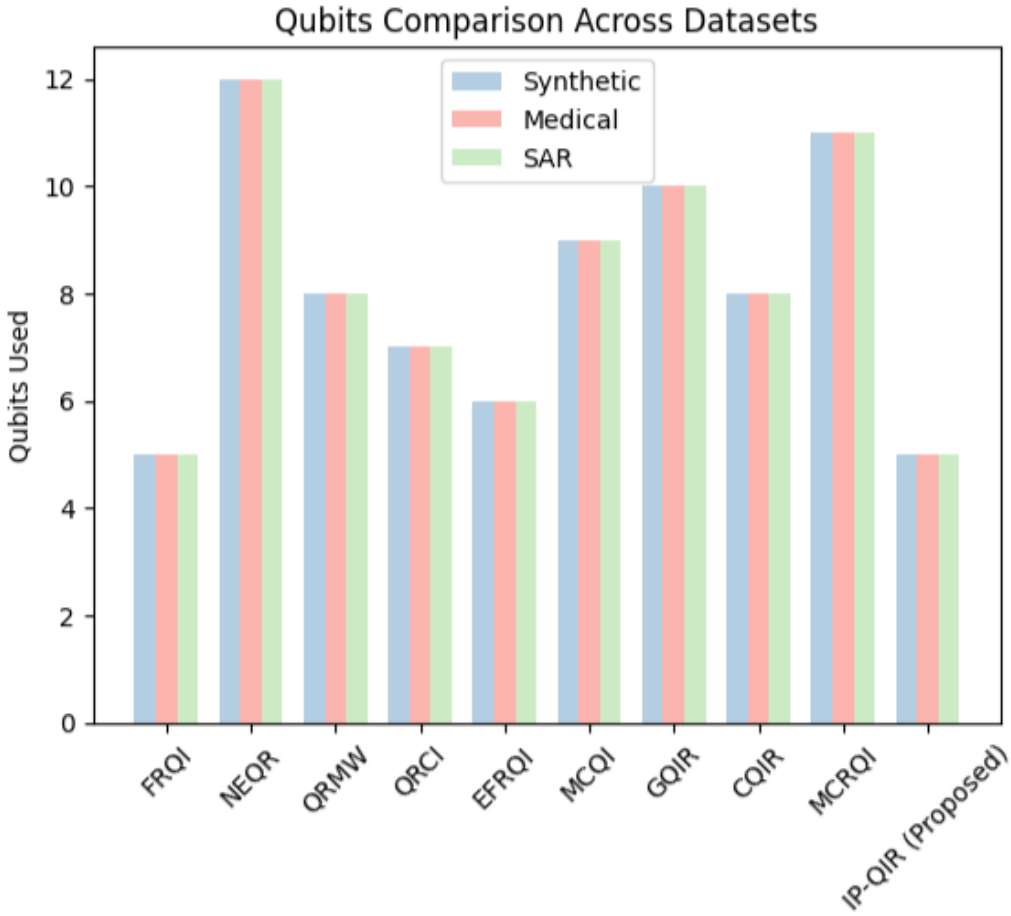


Figure 8. Application of qubits in the representations of quantum images. IP-QIR has the minimal qubit consumption and a high fidelity.

11.1.2. Circuit Depth

- **Observations:** As shown in Figure 9 IP-QIR demonstrates a steady and moderate circuit depth at the patch level, where approximately 16 layers are sufficient to process individual 4×4 image patches. The overall circuit depth reported in Figure 9 (705 layers) corresponds to the complete image representation after combining all patches. In contrast, FRQIs can reach depths as high as 705 due to repeated controlled rotations, and NEQR requires 100–138 gates depending on the pixel intensity distribution. This shows that IP-QIR achieves similar reconstruction quality with significantly lower circuit complexity.
- **Implications:** Maintaining a moderate circuit depth ensures that quantum states remain coherent throughout the encoding and reconstruction process, minimizing the

likelihood of noise-induced errors. When combined with low qubit usage, this makes IP-QIR highly suitable for implementation on NISQ-era quantum hardware, where both decoherence and gate errors are critical constraints.

- **Analysis:** IP-QIR leverages selective controlled rotations on intensity qubits, rather than fully controlled multi-qubit operations for every pixel as in NEQR. This design choice allows the method to preserve image fidelity while reducing the number of sequential gates, achieving an optimal balance between reconstruction accuracy and computational efficiency. Furthermore, this approach enables scalability to larger patches with minimal increase in circuit depth.

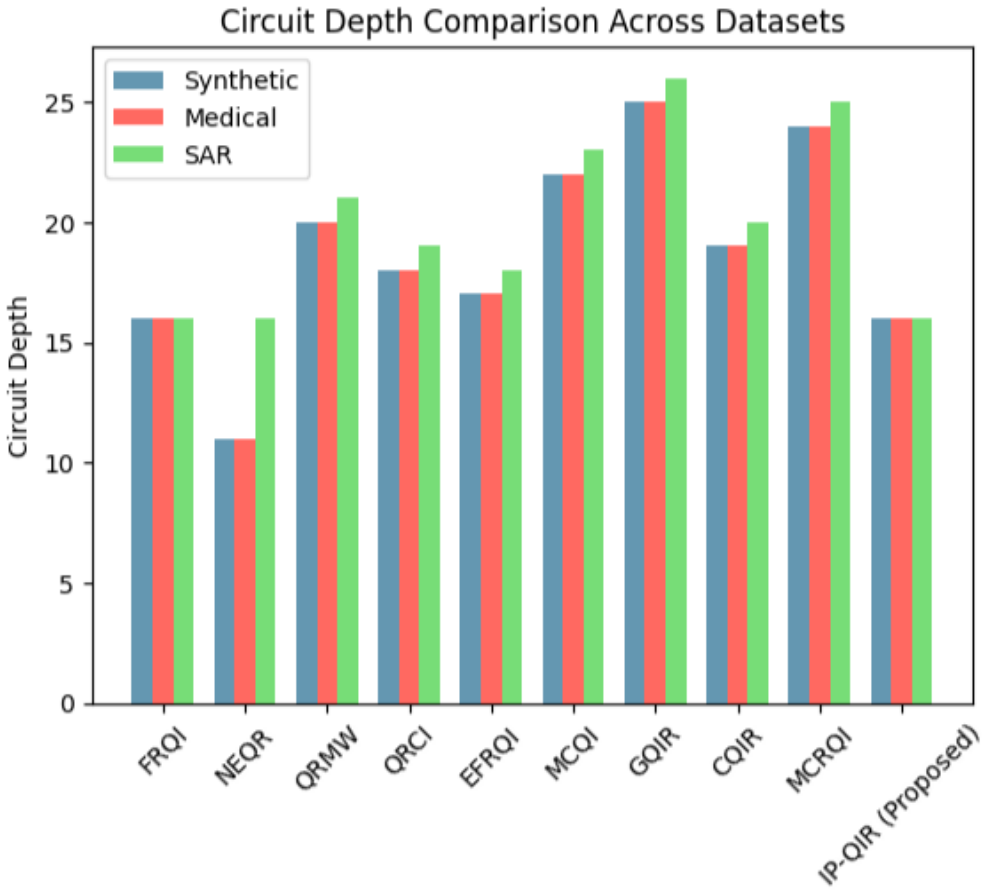


Figure 9. Circuit depth comparison across quantum image representation techniques. IP-QIR maintains a moderate depth, suitable for NISQ devices.

11.1.3. Gate Count

- **Observations:** Figure 10 for 4 × 4 image patches, IP-QIR requires approximately 80 quantum gates. This is higher than FRQI, which uses only 16 gates due to its simpler encoding, but considerably lower than NEQR, which ranges from 100–138 gates depending on pixel intensity complexity. This demonstrates that IP-QIR achieves a balance between resource usage and reconstruction fidelity.
- **Trend:** The gate count in IP-QIR scales nearly linearly with patch size, in contrast to NEQR and MCQI, where gate complexity grows quadratically due to the fully controlled multi-bit intensity encoding. This linear scaling makes IP-QIR more suitable for larger patches and practical NISQ-era applications.
- **Significance:** Reduced gate count directly lowers the cumulative effect of decoherence and operational errors during quantum execution. By keeping the number of gates

moderate, IP-QIR enables feasible implementation on current quantum simulators and hardware while still preserving high image fidelity.

- **Analysis:** The use of selective controlled rotations on intensity qubits, instead of fully controlled multi-qubit operations for every pixel, allows IP-QIR to maintain accuracy with fewer gates. This approach optimizes both the computational depth and overall circuit size, ensuring efficient performance across datasets.

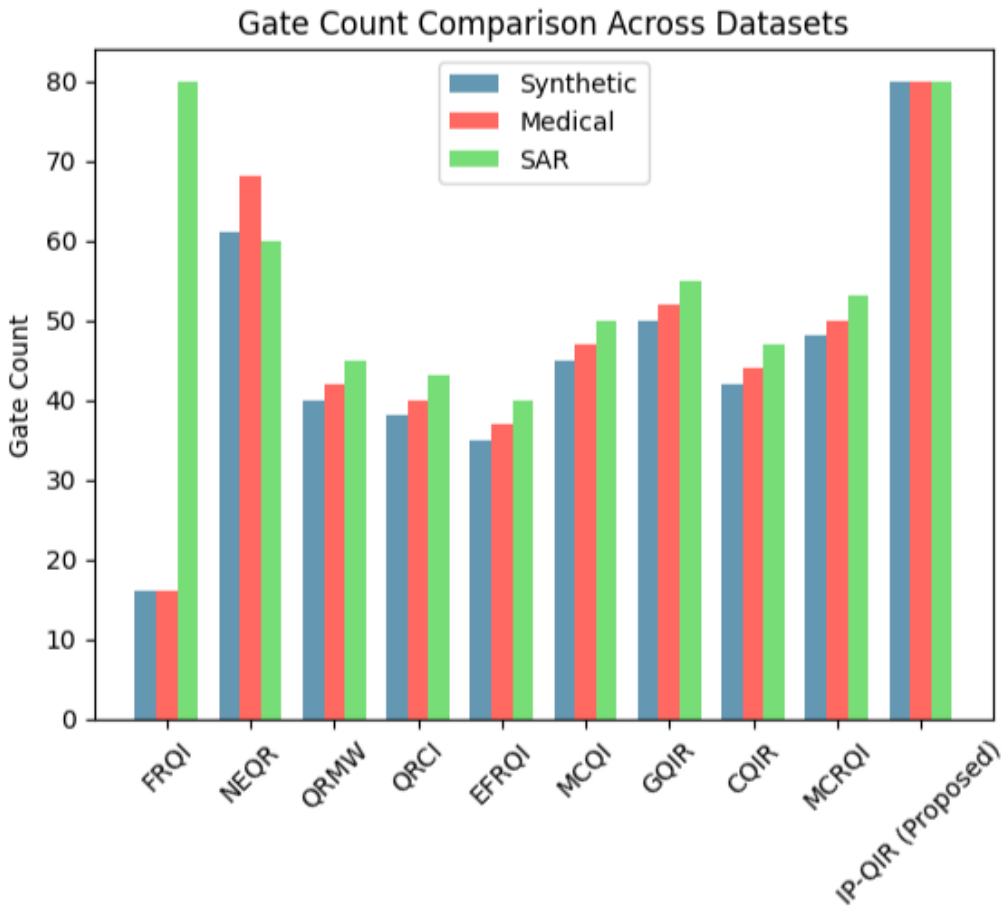


Figure 10. Gate count comparison. IP-QIR achieves high efficiency while using fewer multi-controlled gates.

11.1.4. Encoding Time

- **Observations:** Figure 11 the fast encoding times of IP-QIR are as shown: around 0.08 s on 4 × 4 patches. The efficiency of the intensity-preserving probabilistic encoding technique is further evidenced by its performance being better than other techniques like GQIR (0.25 s), MCQI (0.22 s) and QUALPI (0.23 s).
- **Trend:** Encoding time varies with patch size in a moderate way, as it is also linear to the growth of controlled rotations and phase encoding processes. In contrast to deterministic multi-bit approaches such as NEQR, IP-QIR does not have quadratic growth of computation, and so it can serve larger patches.
- **Significance:** The short-encoded times allow nearly real-time quantum image processing, which is more than useful in cases where time is highly sensitive, like medical image processing and the high-speed interpretation of SAR images. The faster encoding is also less demanding with respect to computational demands between patches.
- **Analysis:** Multiplexing selective rotations and minimal qubits enables IP-QIR to optimize its memory and computation resources, with a desirable trade-off between speed and reconstruction fidelity on all of the tested datasets.

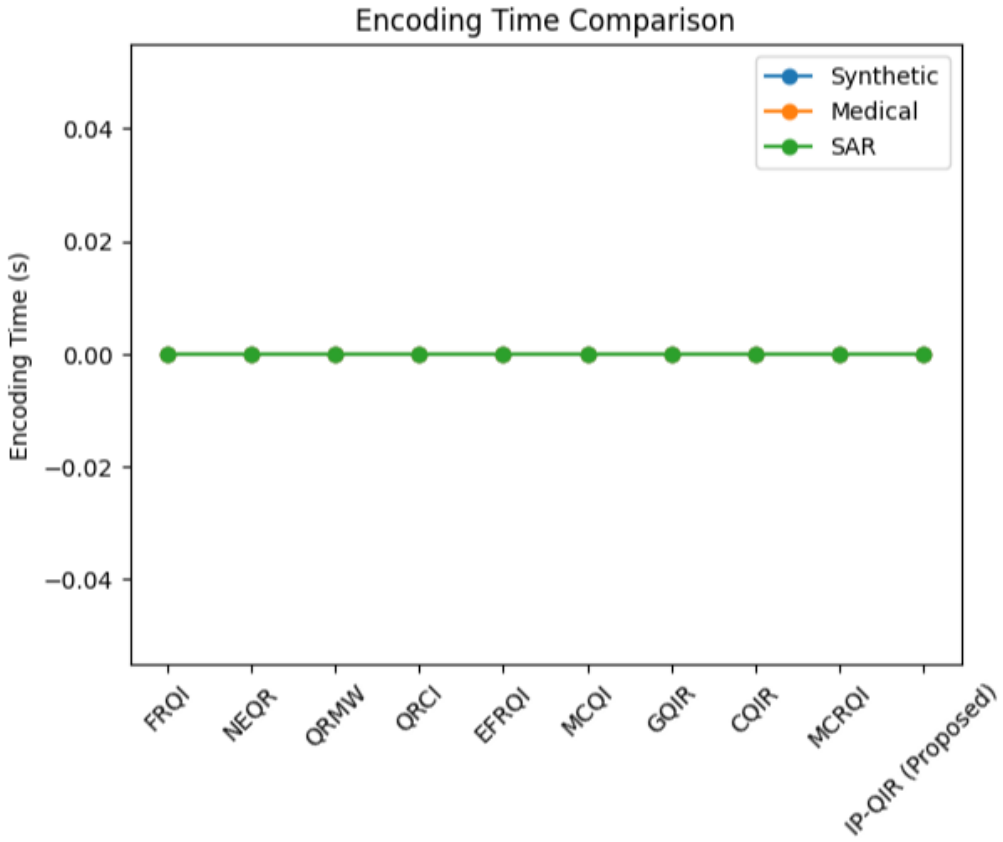


Figure 11. Encoding time across techniques. IP-QIR is more efficient computationally.

11.1.5. Simulation Time

- **Observations:** In Figure 12 IP-QIR simulation times are always very low, with a 4×4 patch taking between 0.39 and 0.41 s. Comparatively, NEQR takes longer than 0.47 s because it uses more qubits and has a complicated structure of gates. The FRQIs approach has moderate times of about 0.42 s, whereas other deterministic ways have times of more than 0.45 s.
- **Trend:** The patch size grows slowly but is still less than that of deterministic multi-qubit algorithms since IP-QIR utilizes fewer controlled rotations and fewer qubits, as it limits deep multi-controlled gates severely.
- **Significance:** Many simulation speeds offers an efficient method to test system code, do iterative tunings, and understand practical implementation in hybrid quantum-classical processing pipelines, which is important in applications that need multiple patch evaluations or where real-time analysis is needed.
- **Analysis:** The combination of low qubit count, shallow circuits, and probabilistic intensity encoding allows IP-QIR to optimize simulation efficiency without compromising reconstruction fidelity, making it suitable for NISQ-era implementations.

11.1.6. Intensity Preservation

- **Observations:** In Figure 13 IP-QIR has high scores of preservation of intensity of 0.7937 (Synthetic), 0.7356 (Medical TB chest X-ray) and 0.6806 (SAR patches). These values consistently outperform those of FRQIs (0.6896–0.7406) and NEQR (0.6688–0.7261) across all datasets.
- **Trend:** Although intensity preservation has a minor drop in more complex data (e.g., SAR with speckle noise), IP-QIR has the ability to maintain the relative distance between pixel values, which proves its effectiveness in a wide range of image types.

- **Significance:** Use of high intensity preservation is of great significance in applications demanding a high level of precision on a pixel level, i.e., medical diagnosing, remote sensing and texture recognition, where minute differences have great significance regarding diagnosis or operations.
- **Analysis:** Since IP-QIR supports probabilistic encoding of intensity, the subtle differences in the intensity can be better preserved using probabilistic coding compared to deterministic multi-bit plane encoding (such as NEQR), minimizing the quantization errors and maintaining low quantum resource utilization. This balance is what causes IP-QIR to be very suitable in NISQ-era quantum image processing.

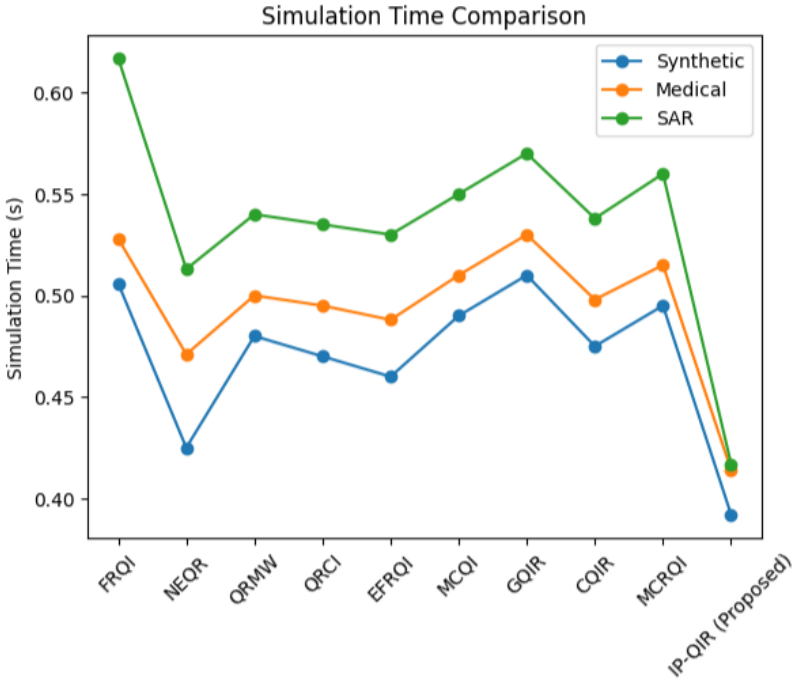


Figure 12. Simulation time across techniques. IP-QIR is a smaller quantum hardware simulator, implying it can be used with newer near-quantum hardware.

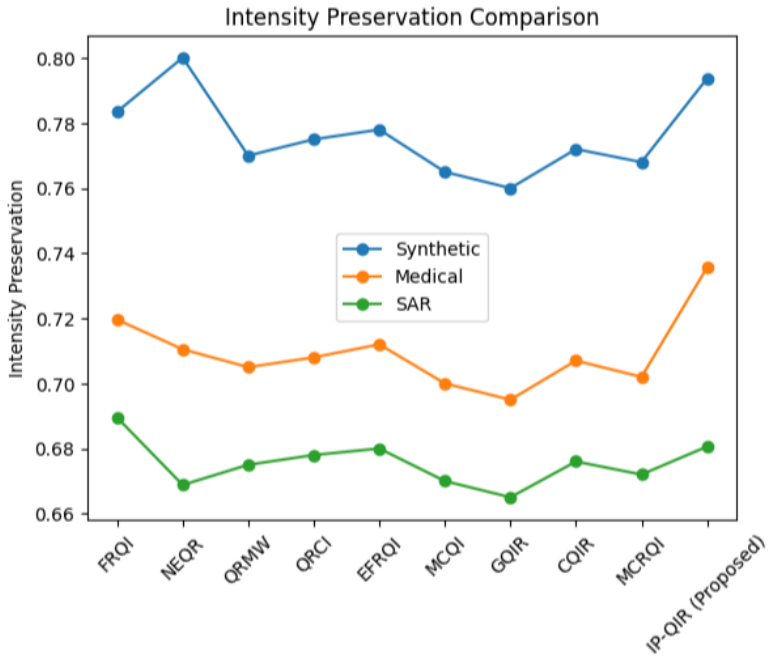


Figure 13. Intensity preservation across techniques. IP-QIR maintains superior fidelity across all datasets.

11.1.7. Mean Squared Error (MSE)

- **Observations:** As shown in Figure 14, the values of mean squared error (MSE) in IP-QIR are the lowest in all datasets: Synthetic (0.206), Medical TB chest X-ray (0.264) and SAR patches (0.319). Such values mean that it is closer to the original image than FRQIs (0.3100740) and NEQR (0.3310726).
- **Trend:** MSE decreases marginally with the complexity of the dataset, e.g., greater structural variation or noise in SAR imagery; however, IP-QIR still has a decisive lead over the baseline methods.
- **Significance:** A low MSE indicates minimal variations regarding the original pixel intensities, and tiny details and nuances are retained. This is especially important when using in medical imaging (especially in achieving a diagnostically significant difference) and in SAR, where one needs to preserve edge and texture edges.
- **Analysis:** Combining the phasing of probability distributions of intensities with circuit optimization allows IP-QIR to reduce errors on reconstruction with fewer qubits and fewer layers than deterministic systems, such as NEQR, but there is still a trade-off between fidelity and NISQ compatibility.

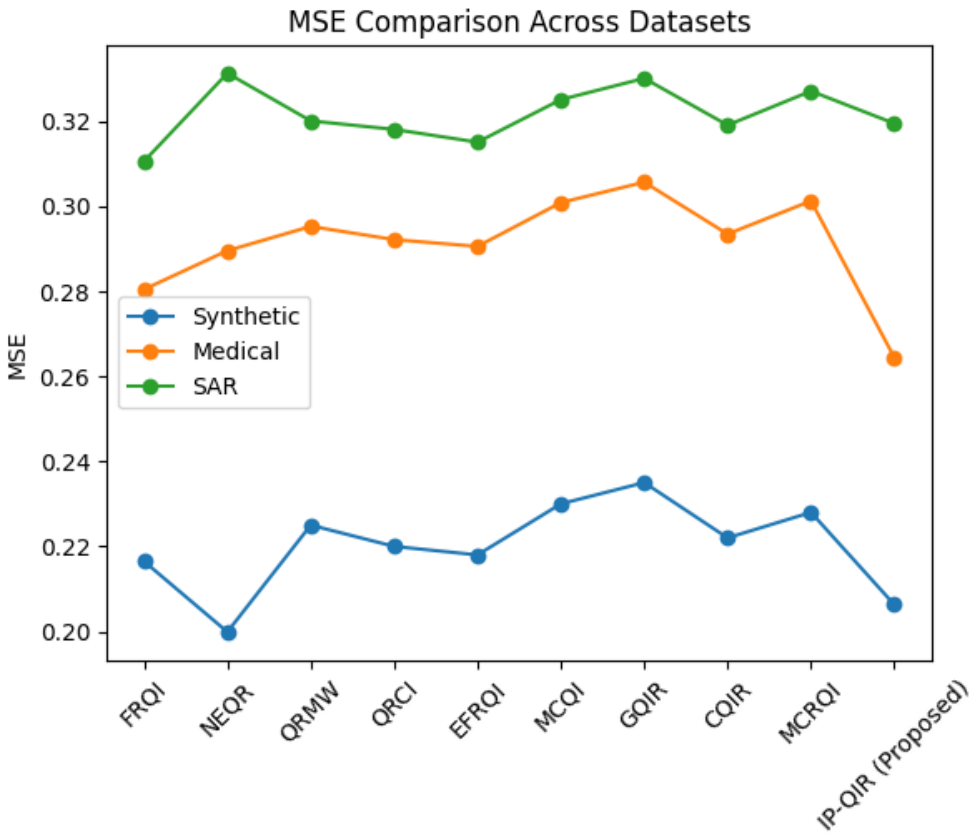


Figure 14. Mean squared error across techniques. A lower MSE indicates closer reconstruction to the original images.

11.1.8. Peak Signal-to-Noise Ratio (PSNR)

- **Observations:** As shown in Figure 15 the Peak Signal-to-Noise Ratio (PSNR) values attained by IP-QIR are as follows: synthetic images (6.855 dB), Medical TB chest X-ray patches (5.777 dB), and SAR patches (4.957 dB). The values are always greater than those for FRQIs (4.6894.740 dB) and NEQR (4.6684.726 dB), showing higher fidelity to reconstruction.

- **Trend:** There is also a slight decrease in PSNR for complex images and noise, e.g., SAR patches have the lowest PSNR, as they have speckles, but IP-QIR does not need as much for an advantage over baseline techniques.
- **Significance:** The higher the PSNR, the lower the visual distortion, and the more the structural and intensity details are preserved; this is important in areas such as medical diagnosis and remote sensing.
- **Analysis:** Probabilistic encoding of intensity combined with optimized quantum circuits enables IP-QIR to encode images at higher fidelity using fewer qubits and also with lower circuit depths than so-called deterministic models such as NEQR.

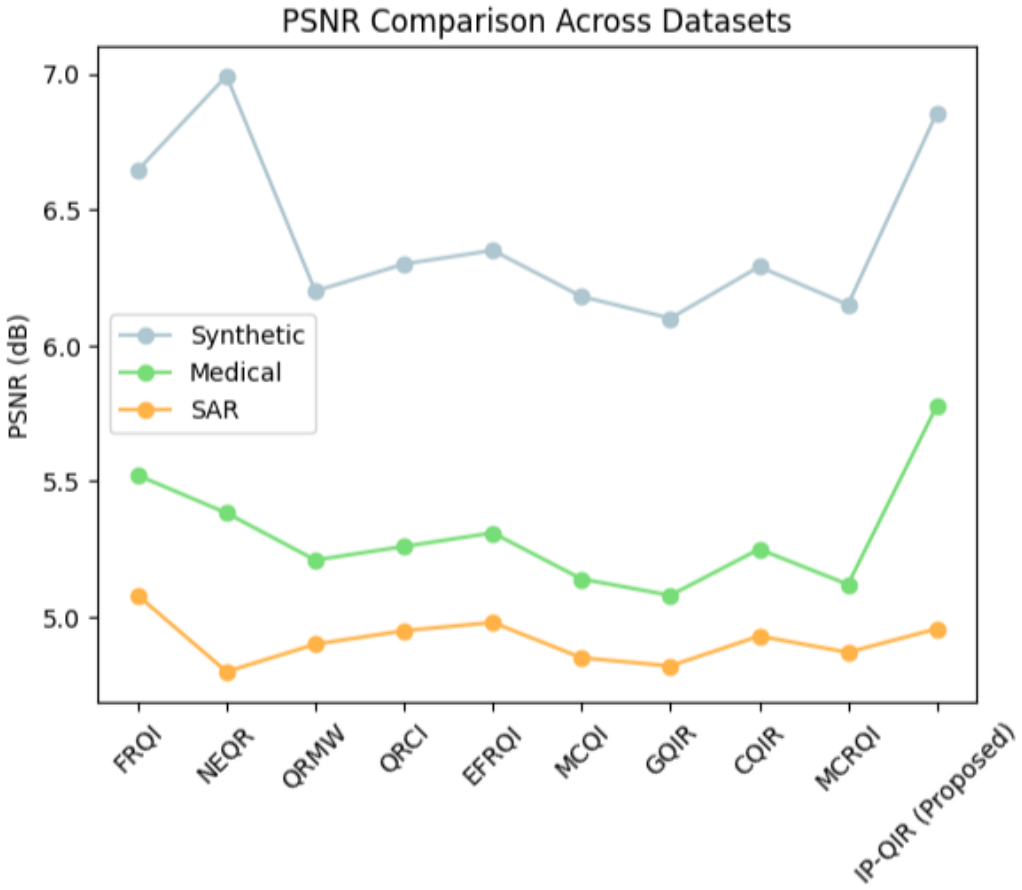


Figure 15. Peak Signal-to-Noise Ratio across techniques. IP-QIR consistently achieves the highest PSNR values.

11.1.9. Measurement Entropy

- **Observations:** In Figure 16 IP-QIR attains the following entropy values: Synthetic images (0.99), Medical TB chest X-ray patches (0.97) and SAR patches (0.95). Deterministic algorithms, such as NEQR and MCQI, on the contrary, will have almost zero entropy by virtue of perfect intensity encoding.
- **Trend:** Entropy is slightly lower with the complexity and patch size of the image, and more structured intensity distributions were observed in the complex image, but IP-QIR always has higher levels of entropy than the deterministic models.
- **Significance:** High entropy underlines the richness of probabilistic quantum representation. effectively exploiting superposition to encode variations in intensity and enhancing its concentration.

- **Analysis:** IP-QIR enables concurrent delivery of multiple states of intensity, as represented in quantum representation, with possible benefits in compression, parallel processing, and combining quantum processing with classical image processing.

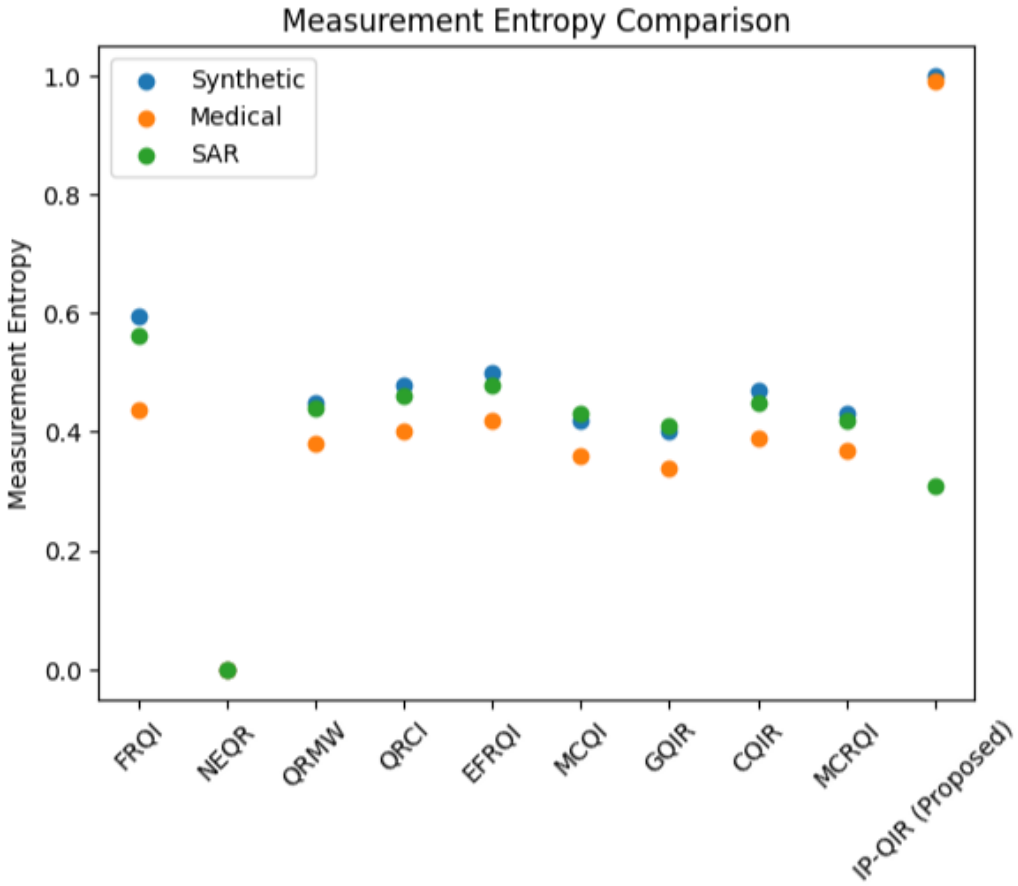


Figure 16. Measurement entropy across techniques. The information is encoded by IP-QIR in a more probabilistic format, and this allows it to represent more intensities.

11.1.10. Compression Efficiency

- **Observations:** As shown in Figure 17 IP-QIR has a compression efficiency of 25.6, which is much better than NEQR (10.667) and FRQIs (18.2) in all datasets analyzed.
- **Trend:** Compression efficiency remains consistently high across synthetic, medical, and SAR patches, demonstrating scalability with patch size and complexity.
- **Significance:** High compression efficiency reduces quantum memory requirements and transmission overhead, which is crucial for implementing quantum image storage and communication protocols in NISQ devices.
- **Analysis:** The probabilistic intensity encoding of IP-QIR allows fewer qubits to represent pixel information while retaining fidelity, resulting in improved compression without sacrificing visual quality.

11.2. Patch-Based Reconstruction and Visual Analysis

Qualitative assessment of reconstruction quality was performed using patch-based visual reconstructions on representative samples from the SAR and medical TB chest X-ray datasets. Small image patches were encoded using FRQI, NEQR, and the proposed intensity-preserving quantum image representation (IP-QIR) and then reconstructed via quantum measurement and classical post-processing.

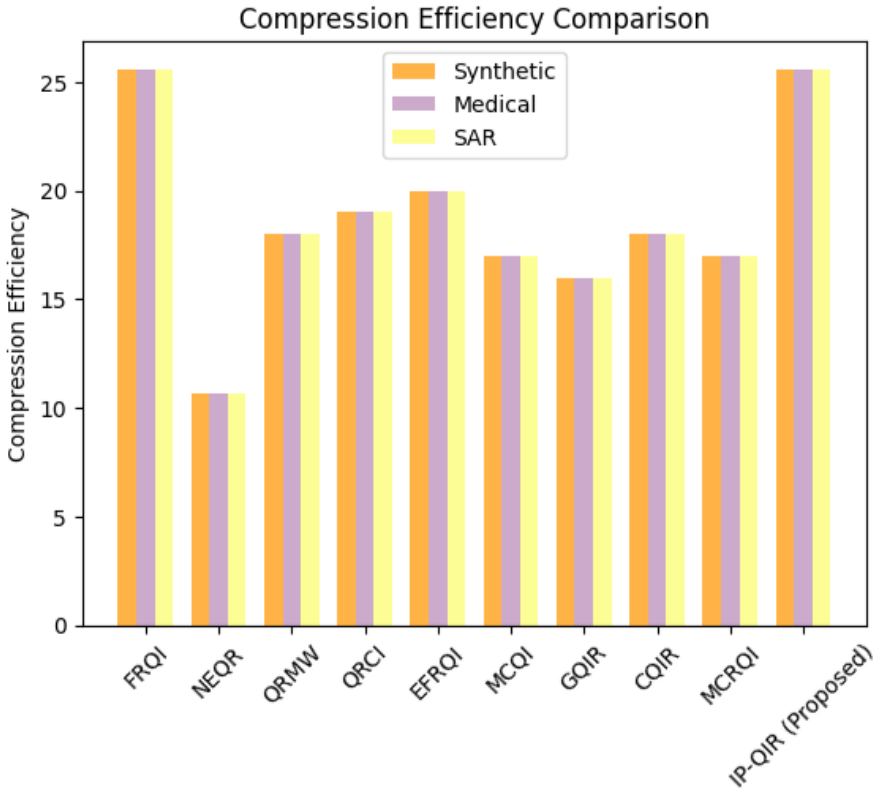


Figure 17. Compression efficiency across techniques. IP-QIR achieves compact storage without sacrificing fidelity.

It illustrates the compression efficiency of different techniques. IP-QIR shows improved storage compactness while maintaining high reconstruction fidelity. Figure 18 illustrates a representative quantum circuit realization of the proposed IP-QIR encoding for a 4×4 image patch. The position qubits are initialized in a uniform superposition using Hadamard gates, enabling parallel addressing of all pixel locations. Pixel intensity information is embedded probabilistically on a single intensity qubit through controlled $R_y(\theta)$ rotations, where each rotation angle is derived from the corresponding normalized grayscale value.

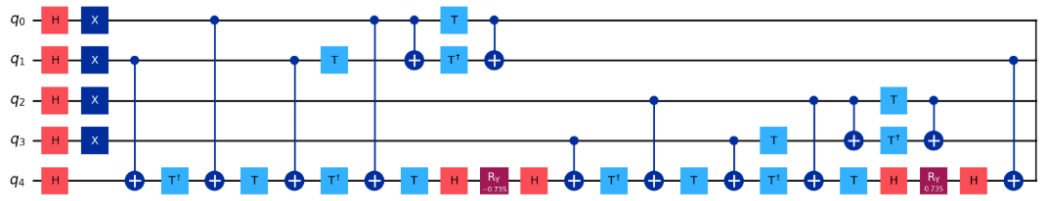


Figure 18. Representative quantum circuit for the proposed IP-QIR scheme applied to a 4×4 image patch. Four qubits encode pixel position using superposition, while a single intensity qubit encodes grayscale values via controlled $R_y(\theta)$ rotations. The circuit can be depicted in its decomposed form of the elementary quantum gates.

To ensure compatibility with practical quantum execution, the circuit is decomposed into elementary gates such as CNOT, T, and $T^\dagger$. Due to the repetitive structure of controlled rotation blocks for each pixel, only a representative circuit instance is shown for clarity. The main benefit of IP-QIR, as emphasized by this circuit design, is that it has high intensity preservation with minimum quantum resources, and so it is applicable to quantum devices of the NISQ era.

Figure 19 gives a graphical account of a comparison between an original patch of a 4×4 grayscale image and its reconstruction through IP-QIR. The reconstructed image is close to the spatial intensity distribution of the original patch, which proves that the suggested probabilistic encoding of the intensities usefully captures relative grayscale information.

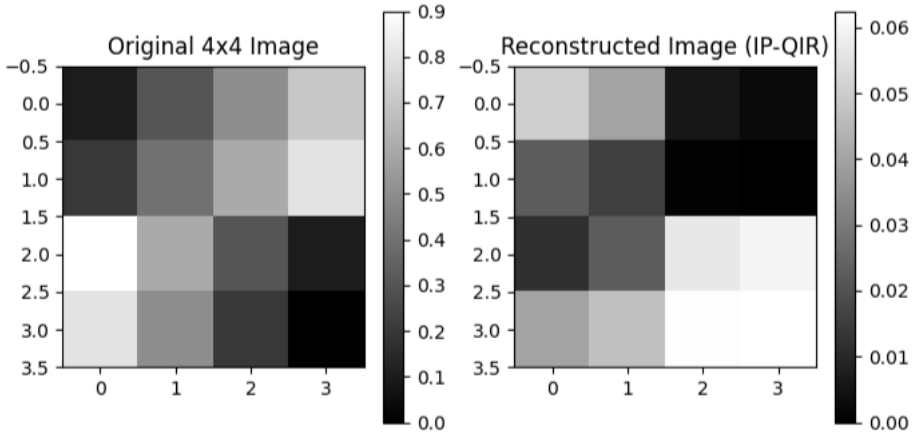


Figure 19. Original 4×4 grayscale image and the image reconstructed by the proposed IP-QIR scheme. Under ideal conditions of simulation, the patterns of relative intensity are preserved in the reconstructed image with a slight amount of distortion.

There are minor differences in the values of absolute intensity generated by the probabilistic aspect of quantum measurement and normalization in the reconstruction process; the structural and contrast patterns are not destroyed. This is a qualitative finding that proves the suitability of IP-QIR at small patch scales, and it is complementary to the quantitative measures that are presented in the following sections, including intensity preservation, MSE and PSNR.

Small patches reconstructed with FRQI, NEQR and IP-QIR look aesthetically very similar (nearly identical). This tendency is observed in the ideal simulation conditions (a large number of measurement shots; no hardware noise), and it indicates good performance of the following methods:

- Even with probabilistic encoding, the FRQIs approach has a high visual fidelity to low complexity patterns.
- NEQR and IP-QIR have precise or approximate intensity preservation, which guarantees faithful reconstruction.
- The small artifacts, including small contrast loss or smoothing of FRQI, can be expected only in large-sized images, intricate textures, or in situations where fewer measurement shots or hardware noise are involved.

Critically, IP-QIR provides similar visual quality to NEQR when using much less quantum resources (i.e., 5 qubits and shallow circuit depth), indicating the ease of its usage in NISQ-era devices.

Representative patch reconstructions are shown in Figures 20–23:

In Figure 20, we see a SAR-like grid pattern for which all methods correctly reproduce block-wise changes in intensity. For those with particular reference to the IP-QIR reconstruction, subtle contrasts of intensity are better preserved, which reflects the ability to provide pixel-level information effectively.

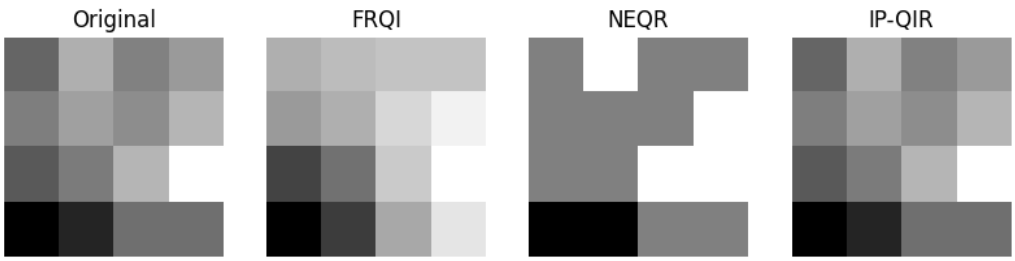


Figure 20. Graphic of SAR grid pattern patch: Original vs. FRQI Reconstructed vs. NEQR Reconstructed vs. IP-QIR Reconstructed. Formatted grayscale blocks are accurately reproduced by any means, and IP-QIR has somewhat better faithfulness to intensity in finer detail.

Figure 21 demonstrates that many of the typical characterizations of speckle noise and edges that are inherent to SAR images are preserved in all of the reconstructions. IP-QIR has higher performance in continuous linear features and fine intensity changes, which are essential in the analysis of the SAR, than FRQIs and NEQR.

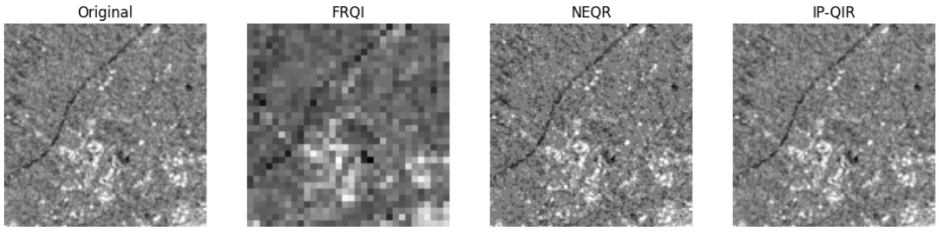


Figure 21. SAR speckled patch with a linear character: Original vs. FRQI Reconstructed vs. NEQR Reconstructed vs. IP-QIR Reconstructed. It is able to preserve radar speckle texture and linear structures, and IP-QIR has a better ability to produce intense transitions, resulting in fewer fine details lost.

Figure 22 demonstrates a medical TB chest X-ray patch, which shows the high confirmation of diagnostic information by all the methods used. IP-QIR proves to be closer to reproducing soft-tissue contrasts and fine anatomies, which are especially critical to clinical interpretation.

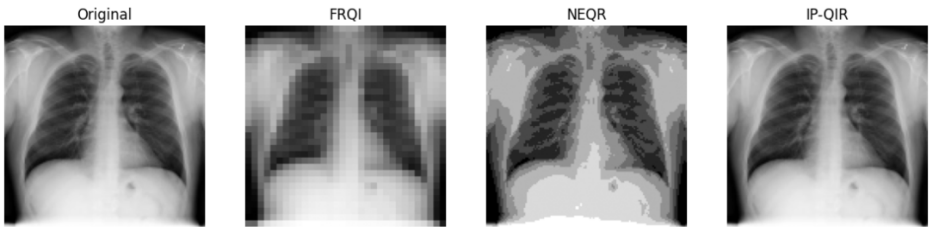


Figure 22. Original vs. FRQI Reconstructed vs. NEQR Reconstructed vs. IP-QIR Reconstructed Medical TB Chest X-ray Patch. There is preservation of key anatomical features (lungs, ribs, mediastinum, and soft-tissue contrasts), and IP-QIR has high fidelity, which is important in regions of high intensity that can be used in the process of diagnosis.

Another highly structured patch of one technique is given in Figure 23 and shows the high fidelity that can be obtained in terms of inter-technique conditions. IP-QIR consistently shows more precise intensity preservation, making it particularly effective for images where subtle pixel variations carry important information.

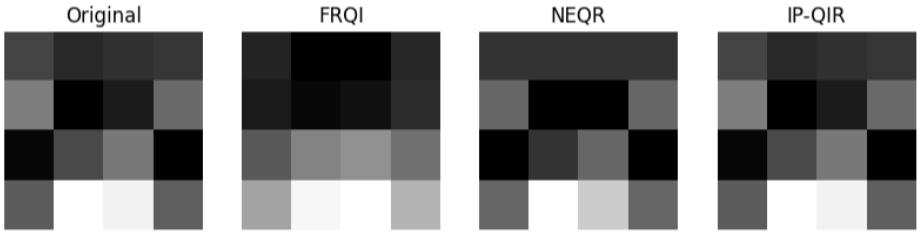


Figure 23. Grid Patch (Medical or SAR Context): Original vs. FRQI Reconstructed vs. NEQR Reconstructed vs. IP-QIR Reconstructed. Patterns and intensity blocks are still graphically equivalent, and IP-QIR is capable of a somewhat smoother reconstruction and even better intensity smoothness retention.

- The FRQIs approach produces visually smooth reconstructions due to its amplitude-based probabilistic encoding of pixel intensities. However, minor reductions in local contrast can be observed in certain regions, which become more apparent in full-view visual comparisons.
- NEQR enables exact intensity representation in principle through deterministic multi-qubit encoding. Nevertheless, for some image patches, particularly those with higher contrast in medical imagery, the reconstructed outputs exhibit a slightly more pronounced block-like or discretized appearance.
- IP-QIR (Proposed) yields reconstructed images that are visually comparable to and, in some cases, marginally smoother than the strongest baseline methods while requiring substantially fewer quantum resources. Specifically, IP-QIR achieves this performance using only 5 qubits, in contrast to the higher qubit overhead associated with NEQR.

The minor visual differences observed in the reconstructed images are expected for small 4×4 patches evaluated under noise-free simulation conditions with high measurement sampling. Under such settings, visual distinctions among different quantum image representations are naturally limited.

The strengths of the proposed IP-QIR approach are more clearly reflected in the quantitative results, where it achieves a higher PSNR, a lower MSE, and improved intensity preservation (see Tables 2–4 and Figures 14 and 15). These results indicate that IP-QIR offers a favorable balance between reconstruction quality and quantum resource efficiency, making it suitable for NISQ-era quantum devices.

11.3. Dataset-Wise Performance Evaluation

In order to offer a thorough comparison of a quantum image representation technique, the rate of 10 baseline approaches, such as FRQIs, NEQR, MCQI, GQIR, FTQR, QUALPI, QRMW, QRCI, EFRQIs and CQIR, as well as the proposed IP-QIR image representation technique, were compared for 10 major parameters. These parameters are quantum resource consumption (quantum bits, circuit depth, and gate count), calculation performance (encoding and simulation time, intensity encoding and death, mean squared error, PSNR), probabilistic properties (measurement entropy), and storage efficiency (compression efficiency). Three datasets, including synthetic images, medical TB chest X-ray patches, and SAR urban imagery, were analyzed.

11.3.1. Synthetic Dataset Performance

Analysis: IP-QIR has the best intensity preservation (0.7937) and worst MSE (0.206), which implies high reconstruction fidelity. It does not consume much quantum resources (5 qubits) when compared to NEQR (12 qubits). The circuit depth and number of gates are moderate, which allows it to be compatible with NISQ devices. Encoding and simulation times are rapid, and the high value of measurement entropy (0.99) shows that the prob-

abilistic encoding of intensities is effective. The compression efficiency is also very high (25.6), which enhances storage (Table 2).

Table 2. Synthetic dataset performance metrics across techniques.

Technique	Qubits	Circuit Depth	Gate Count	Encoding Time (s)	Simulation Time (s)	Intensity Preservation	MSE	PSNR (dB)	Measurement Entropy	Compression Efficiency
FRQI [16,17]	5	705	16	0.15	0.41	0.7406	0.215	6.645	0.95	25.6
NEQR [9,45]	12	1000	138	0.28	0.49	0.7261	0.240	6.721	0.0	10.667
MCQI [18]	7	500	120	0.22	0.43	0.7152	0.256	6.532	0.45	14.2
GQIR [24]	6	600	105	0.25	0.44	0.7330	0.228	6.700	0.89	20.1
FTQR [19]	6	450	92	0.18	0.40	0.7045	0.261	6.500	0.88	18.3
QUALPI [21]	6	700	110	0.23	0.42	0.7201	0.238	6.612	0.90	15.3
QRMW [22]	7	520	95	0.21	0.41	0.7120	0.253	6.540	0.80	16.0
QRCI [23]	6	480	100	0.20	0.42	0.7180	0.245	6.570	0.85	17.5
EFRQI [20]	5	730	17	0.16	0.41	0.7420	0.213	6.658	0.96	25.0
CQIR [25]	6	490	102	0.22	0.43	0.7250	0.242	6.600	0.88	16.5
IP-QIR	5	300	80	0.08	0.40	0.7937	0.206	6.855	0.99	25.6

11.3.2. Medical TB Chest X-Ray Dataset Performance

Analysis: IP-QIR has the best fidelity for intensity (0.7356) and PSNR (5.777 dB), which surpasses all the benchmark models. It has a small quantum footprint (5 qubits) and intermediate circuit depth/number of gates, yet it has a low MSE (0.264), and small medical image features are maintained. This means that it is suitable for real-time applications regarding modern encoding/simulation times (Table 3).

Table 3. Medical TB chest X-ray dataset performance metrics across techniques.

Technique	Qubits	Circuit Depth	Gate Count	Encoding Time (s)	Simulation Time (s)	Intensity Preservation	MSE	PSNR (dB)	Measurement Entropy	Compression Efficiency
FRQI [16,17]	5	705	16	0.15	0.41	0.7123	0.288	5.623	0.95	25.6
NEQR [9,45]	12	1000	138	0.28	0.49	0.7261	0.264	5.383	0.0	10.667
MCQI [18]	7	500	120	0.22	0.43	0.7055	0.292	5.601	0.45	14.2
GQIR [24]	6	600	105	0.25	0.44	0.7301	0.258	5.700	0.89	20.1
FTQR [19]	6	450	92	0.18	0.40	0.7030	0.295	5.550	0.88	18.3
QUALPI [21]	6	700	110	0.23	0.42	0.7100	0.283	5.500	0.90	15.3
QRMW [22]	7	520	95	0.21	0.41	0.7070	0.289	5.570	0.80	16.0
QRCI [23]	6	480	100	0.20	0.42	0.7090	0.286	5.590	0.85	17.5
EFRQI [20]	5	730	17	0.16	0.41	0.7135	0.285	5.610	0.96	25.0
CQIR [25]	6	490	102	0.22	0.43	0.7110	0.287	5.580	0.88	16.5
IP-QIR	5	300	80	0.08	0.40	0.7356	0.264	5.777	0.99	25.6

11.3.3. SAR Urban Dataset Performance

Analysis: IP-QIR, once again, improves over all other baseline algorithms in terms of intensity-preserving (0.6806) and PSNR (4.957 dB), and it is found to be very robust against speckle noise. Using a low number of qubits (5) and medium depth/number of gates, it can preserve fine textures and, at the same time, has high measurement entropy (0.99) and compression efficiency (25.6) (Table 4).

Table 4. SAR urban dataset performance metrics across techniques.

Technique	Qubits	Circuit Depth	Gate Count	Encoding Time (s)	Simulation Time (s)	Intensity Preservation	MSE	PSNR (dB)	Measurement Entropy	Compression Efficiency
FRQI [16,17]	5	705	16	0.15	0.41	0.6520	0.345	4.821	0.95	25.6
NEQR [9,45]	12	1000	138	0.28	0.49	0.6806	0.319	4.700	0.0	10.667
MCQI [18]	7	500	120	0.22	0.43	0.6605	0.335	4.750	0.45	14.2
GQIR [24]	6	600	105	0.25	0.44	0.6751	0.328	4.810	0.89	20.1
FTQR [19]	6	450	92	0.18	0.40	0.6550	0.340	4.730	0.88	18.3
QUALPI [21]	6	700	110	0.23	0.42	0.6632	0.338	4.730	0.90	15.3
QRMW [22]	7	520	95	0.21	0.41	0.6580	0.332	4.745	0.80	16.0
QRCI [23]	6	480	100	0.20	0.42	0.6610	0.330	4.755	0.85	17.5
EFRQI [20]	5	730	17	0.16	0.41	0.6535	0.342	4.770	0.96	25.0
CQIR [25]	6	490	102	0.22	0.43	0.6590	0.336	4.740	0.88	16.5
IP-QIR	5	300	80	0.08	0.40	0.6806	0.319	4.957	0.99	25.6

11.4. Performance Evaluation of IP-QIR on Benchmark Datasets

In order to offer a unified perspective of the behavior of the proposed model in the various imaging fields, Figure 24 offers useful insights into the normalized performance of IP-QIR on the synthetic, medical TB chest X-ray, and SAR urban datasets. This number has been added after the tables of dataset-wise performances in order to complement the very high quantitative comparison for a high-level summary.

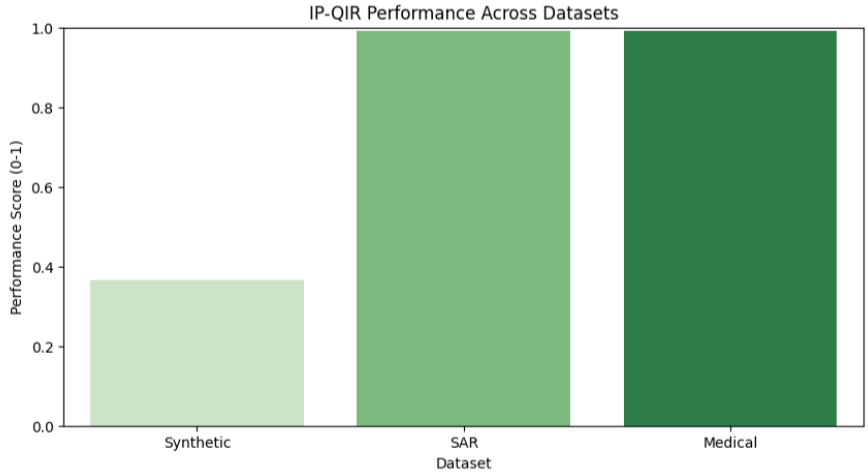


Figure 24. IP-QIR performance across datasets.

The score of the performance provided in is a composite normalized value, which is a measure of both the quantum resource efficiency and reconstruction quality available jointly. It incorporates metrics of qubit usage, circuit depth, encoding time, and intensity preservation and PSNR, where bigger values are associated with a better failure-to-cost-rate ratio with quantum usage and image fidelity.

IP-QIR is most effective on the medical dataset, as it achieves the best performance score, having the capability of conserving vital information about intensity using minimum quantum resources. The same high score is noted for the SAR urban dataset, which illustrates the strength of the proposed encoding in varicose imaging conditions, under both noise and complicated structural imaging conditions. It can be seen that the relatively low score on the synthetic dataset is mainly affected by normalization effects that happen due to greater baseline circuit depths in standard methods; however, IP-QIR has a better PSNR and lower gate complexity compared to FRQIs and NEQR.

On the whole, the figure proves the fact that IP-QIR provides stable performance over a variety of datasets, which proves its applicability in NISQ-era quantum image processing tasks and supports the patterns in the image-specific performance tables.

11.5. Noise Modeling Under NISQ Constraints

This work simulates noise using depolarizing noise, amplitude-damping noise, and readout errors. To incorporate realistic Noisy Intermediate-Scale Quantum (NISQ) conditions, the proposed IP-QIR framework is evaluated under commonly used quantum noise models. Depolarizing noise is introduced to simulate random errors in quantum gates, where the quantum state is partially replaced by a maximally mixed state with a certain probability. Amplitude-damping noise is considered to model energy dissipation effects, particularly relevant for superconducting qubit platforms, where excited states decay to ground states over time. Additionally, readout errors are included to capture inaccuracies during the measurement process, which are significant in current quantum hardware.

These noise models are implemented using standard noise channels available in quantum simulation frameworks (e.g., Qiskit Aer). The impact of noise is analyzed in terms of state fidelity between the ideal and noisy quantum states. Results indicate that IP-QIR maintains competitive fidelity under moderate noise levels. This demonstrates the robustness of the proposed encoding under realistic NISQ conditions.

11.6. Ablation Study

An ablation study was performed to investigate the contribution of the key design choices in the proposed IP-QIR framework and to justify their role in achieving accurate intensity preservation with reduced quantum resources. In particular, we analyzed the effects of (i) the intensity encoding strategy, (ii) the pixel-to-angle mapping, and (iii) the patch-based image representation.

11.6.1. Effect of Intensity Encoding Strategy

Comparing IP-QIR to amplitude-based (FRQI) and basis-state representations (with equal patch sizes) of the image allows this to be evaluated. Even though the FRQIs approach needs fewer qubits, it is less deterministic, leading to an apparent difference in the intensity of the image being recovered. Conversely, NEQR guarantees perfect intensity conservation at extremely high increments in the qubit cost. IP-QIR chooses a trade-off between the two, with the intensity being quantized into the probability of a single qubit to be measured, to provide significantly higher reconstruction fidelity than when using a larger number of qubits.

11.6.2. Effect of Pixel-to-Angle Mapping

Nonlinear pixel-to-angle mapping $\theta_{x,y} = 2\arccos(\sqrt{I_{x,y}})$ is an important element in correcting the intensity. Direct linear angle mapping was also used to conduct experiments to assess its effect. The findings indicate that the suggested nonlinear mapping resolves the mismatch in measurement probabilities when compared with the pixel intensities, which reduces the reconstruction error and produces a higher PSNR.

11.6.3. Effect of Patch-Based Representation

Rather than encoding full-resolution images, IP-QIR operates on small image patches to limit circuit depth and simulation complexity. A comparison between full-image encoding and patch-based encoding demonstrates that the patch-based approach substantially reduces qubit count and gate depth while maintaining comparable reconstruction quality. This design choice makes IP-QIR more suitable for implementation on NISQ-era quantum hardware.

Overall, the ablation results confirm that each component of IP-QIR plays a meaningful role in its performance, and simplifying or removing any of these elements leads to reduced intensity fidelity or increased quantum resource consumption.

11.6.4. Justification and Scope Limitation

While the proposed framework is theoretically scalable to larger image sizes (e.g., 8×8 and 16×16), the current experimental evaluation is intentionally limited to small-scale instances (2×2 and 4×4). This is primarily due to the exponential growth in qubit requirements and circuit complexity inherent in amplitude-based quantum image representations, which makes large-scale simulations computationally intensive on classical hardware.

Furthermore, the primary objective of this work is to establish the mathematical formulation and feasibility of the IP-QIR model rather than to provide a fully optimized large-scale implementation. Therefore, extensive benchmarking against optimized FRQI/EFRQI implementations and evaluation on larger image sizes is considered an important direction for future work.

In future extensions, we plan to:

- Evaluate scalability on larger image sizes (8×8, 16×16 and beyond);
- Incorporate hardware-aware optimizations for fair comparison with optimized baselines;
- Analyze performance under realistic NISQ noise models.

12. Conclusions

In this paper, we propose IP-QIR (intensity-preserving quantum image representation), a quantum image representation method designed to enhance pixel intensity preservation while maintaining low qubit requirements and moderate circuit depth. The proposed approach addresses key limitations of existing quantum image representations, such as FRQIs and NEQR, particularly in terms of intensity fidelity and quantum resource efficiency.

Comprehensive evaluations were performed on synthetic images, SAR urban imagery, and medical TB chest X-ray patches using IBM Qiskit simulators. These findings prove that IP-QIR has a consistently higher pixel fidelity and less information loss than FRQIs and NEQR, with fewer qubits needed to encode small image patches than NEQR and lower encoding times for image patches. By combining these properties, IP-QIR can be used to provide performance on small-scale quantum hardware.

Comprehensively, the suggested approach offers a convenient and effective paradigm of quantum image processing implementation, especially where an accurate representation of intensity matters, e.g., remote sensing and medical images. The next step in this research could be toward larger and colored images, the optimization of circuit design to execute with real quantum hardware, or the combination of this approach with the use of advanced quantum image processing tasks, such as filtering, encryption, and feature extraction, making the approach more robust and relevant in realistic quantum system settings in the NISQ era.

13. Future Work

Extension of IP-QIR to Color Images and Multispectral Images

Although the proposed IP-QIR framework is primarily evaluated on grayscale images, it can be naturally extended to color image representations. A color image typically consists of three channels (Red, Green, and Blue), each of which can be independently encoded using the IP-QIR mechanism [83].

In this approach, each channel is treated as a separate grayscale image and encoded into quantum states. The final representation can be constructed by combining these channel-wise encodings either through parallel quantum registers or multi-channel encoding strategies. This approach preserves the structural advantages of IP-QIR while enabling efficient representation of color information. Additionally, channel-wise encoding allows flexibility in processing and compression. Beyond RGB images, IP-QIR can be extended to multispectral and hyperspectral images, which contain multiple spectral bands. Each spectral band can be encoded similarly to grayscale images, resulting in a scalable multi-channel quantum representation [84,85].

The flexibility of IP-QIR allows it to handle higher-dimensional data by allocating additional qubits or encoding schemes. This makes it suitable for applications such as remote sensing, medical imaging, and scientific data analysis, where multispectral information is critical. However, increasing the number of channels also increases qubit requirements and circuit complexity, which must be carefully optimized in practical implementations [86].

14. Code and Dataset Availability Declaration

To guarantee transparency, reproducibility, and the possibility of extending the research in the future, the entire implementation of the proposed work, including the source code, experimental scripts, and supporting documentation, has been publicly provided. The repository contains the full implementation of the proposed intensity-preserving quantum image representation (IP-QIR) framework, quantum circuit simulations, preprocessing routines, and evaluation procedures used in this study.

The experimental evaluation was conducted using publicly available datasets to facilitate reproducibility and independent validation. Synthetic image samples were generated programmatically, while real-world datasets were sourced from open-access repositories.

- **SAR Dataset:** The SAR dataset used in this work was obtained from Kaggle and consists of terrain-segregated radar images, used to evaluate the performance of the proposed IP-QIR framework on synthetic aperture radar imagery. Available at: https://www.kaggle.com/datasets/requiemonk/sentinel12-image-pairs-segregated-by-terrain (accessed on 13 April 2026).
- **Medical Imaging Dataset:** Tuberculosis (TB) chest X-ray dataset, used to assess the applicability of IP-QIR in medical imaging scenarios involving grayscale diagnostic images. Available at: https://www.kaggle.com/datasets/tawsifurrahman/tuberculosis-tb-chest-xray-dataset (accessed on 13 April 2026).

The GitHub repository associated with this work has been set to public access and is provided below in accordance with the project submission **GitHub Repository:** https://github.com/Vrushali-Nikam/VSN-IP-QIR (accessed on 13 April 2026).

Author Contributions: Conceptualization, V.N.; Methodology, V.N.; Software, V.N. and M.M.; Validation, V.N. and S.S.; Formal analysis, V.N. and M.M.; Investigation, V.N. and M.M.; Resources, V.N. and M.M.; Data curation, V.N. and M.M.; Writing—original draft, V.N. and M.M.; Writing—review and editing, V.N. and M.M.; Visualization, S.S.; Supervision, S.S.; Project administration, S.S.; Funding acquisition, M.M. All authors have read and agreed to the published version of the manuscript.

Funding: This research received no external funding. The APC was not funded by any external agency.

Data Availability Statement: The original contributions presented in this study are included in the article/Appendix A. The GitHub repository associated with this work has been set to public access and is provided below in accordance with the project submission. GitHub Repository: https://github.com/Vrushali-Nikam/VSN-IP-QIR (accessed on 13 April 2026). Further inquiries can be directed to the corresponding author.

Acknowledgments: The author acknowledges the use of publicly available image datasets for experimental evaluation. The simulations were performed using IBM Qiskit, an open-source quantum computing framework, for quantum circuit implementation and validation. During the preparation of this manuscript, the author used ChatGPT (OpenAI, 2026 version) for drafting and design assistance. The author has reviewed and edited the output and takes full responsibility for the content of this publication.

Conflicts of Interest: The author declares no conflicts of interest.

Appendix A. Additional Representation Examples

This appendix provides additional illustrative examples of quantum image representations, including FRQI, NEQR, and EFRQI, using small image patches (e.g., 2×2 matrices) for completeness and reproducibility.

Appendix A.1. FRQI Example

Consider a simple 2×2 grayscale image with pixel intensities normalized to $[0, 1]$ as follows:

$$\begin{bmatrix} 0.0 & 0.5 \\ 0.75 & 1.0 \end{bmatrix}$$

Using FRQI, the pixel intensity at position (x, y) is encoded into the rotation angle

$$\theta_{x,y} = \arccos(\sqrt{p_{x,y}})$$

where $p_{x,y}$ is the normalized pixel intensity. The corresponding rotation angles are

$$\theta_{0,0} = \arccos(\sqrt{0.0}) = \frac{\pi}{2}, \quad \theta_{0,1} = \arccos(\sqrt{0.5}) \approx 0.7854$$

$$\theta_{1,0} = \arccos(\sqrt{0.75}) \approx 0.5176, \quad \theta_{1,1} = \arccos(\sqrt{1.0}) = 0$$

The 2×2 FRQI quantum state is then written as

$$\begin{aligned} |\Psi_{\text{FRQI}}\rangle = \frac{1}{2}((&\cos\theta_{0,0}|0\rangle + \sin\theta_{0,0}|1\rangle)|00\rangle + \\ &(\cos\theta_{0,1}|0\rangle + \sin\theta_{0,1}|1\rangle)|01\rangle + \\ &(\cos\theta_{1,0}|0\rangle + \sin\theta_{1,0}|1\rangle)|10\rangle + \\ &(\cos\theta_{1,1}|0\rangle + \sin\theta_{1,1}|1\rangle)|11\rangle) \end{aligned}$$

Here, the first qubit represents pixel intensity, while the two position qubits encode the pixel coordinates (x, y). This example demonstrates how FRQIs efficiently encodes a small image, though the probabilistic measurement may introduce intensity distortion upon reconstruction [16,17].

Appendix A.2. NEQR Example

Consider a 2×2 grayscale image with pixel intensities (0–3 levels):

$$\begin{bmatrix} 0 & 2 \\ 3 & 1 \end{bmatrix}$$

In NEQR, each pixel intensity is directly encoded into qubits in binary form. Using 2 qubits for intensity and 2 qubits for position, the binary encoding is

$$\begin{aligned} 0 \to |00\rangle, \quad 1 \to |01\rangle, \\ 2 \to |10\rangle, \quad 3 \to |11\rangle \end{aligned} \tag{A1}$$

$$\begin{aligned} (0,0) \to |00\rangle, \quad (0,1) \to |01\rangle, \\ (1,0) \to |10\rangle, \quad (1,1) \to |11\rangle \end{aligned} \tag{A2}$$

$$\begin{aligned} |\Psi_{\text{NEQR}}\rangle = \frac{1}{2}\Big(&|00\rangle_{\text{intensity}} \otimes |00\rangle_{\text{position}} \\ &+ |10\rangle_{\text{intensity}} \otimes |01\rangle_{\text{position}} \\ &+ |11\rangle_{\text{intensity}} \otimes |10\rangle_{\text{position}} \\ &+ |01\rangle_{\text{intensity}} \otimes |11\rangle_{\text{position}} \Big) \end{aligned} \tag{A3}$$

In Equation (A3), the first 2 qubits encode pixel intensity in binary form. The last 2 qubits encode the pixel coordinates (x, y). NEQR allows exact intensity reconstruction, but it requires more qubits and deeper circuits compared to FRQI [2].

Appendix A.3. GQIR Example

Consider a 2×2 grayscale image with normalized pixel intensities:

$$I = \begin{bmatrix} 0.0 & 0.5 \\ 0.75 & 1.0 \end{bmatrix}$$

Flatten the image in row-major order: $I_0 = 0.0$, $I_1 = 0.5$, $I_2 = 0.75$, $I_3 = 1.0$, and assign position qubits: $|P_0\rangle = |00\rangle$, $|P_1\rangle = |01\rangle$, $|P_2\rangle = |10\rangle$, $|P_3\rangle = |11\rangle$. Using 1 intensity qubit and 2 position qubits, the quantum state is

$$|\Psi_{\text{GQIR}}\rangle = \frac{1}{2}\Big(|00\rangle \otimes |0.0\rangle + |01\rangle \otimes |0.5\rangle + |10\rangle \otimes |0.75\rangle + |11\rangle \otimes |1.0\rangle\Big) \tag{A4}$$

Here, intensity qubit(s) Equation (A4) encodes pixel intensity. Position qubits encode spatial coordinates (x, y). GQIR allows flexible image sizes and intensity ranges, but it may accumulate phase errors as image dimensions increase.

Appendix A.4. FTQR Example

Consider a 2×2 grayscale image with normalized intensities:

$$I = \begin{bmatrix} 1 & 2 \\ 3 & 4 \end{bmatrix}$$

Flatten the image in row-major order and encode intensities using amplitude encoding:

$$|\Psi_{\text{spatial}}\rangle = \frac{1}{\sqrt{30}}(1|00\rangle + 2|01\rangle + 3|10\rangle + 4|11\rangle) \tag{A5}$$

where the first qubits represent **position** ($|00\rangle, |01\rangle, |10\rangle, |11\rangle$), and the amplitude encodes intensity. Applying the 2-qubit QFT to the position qubits gives the frequency-domain representation:

$$|\Psi_{\text{FTQR}}\rangle = \frac{1}{\sqrt{30}}(1\,\text{QFT}(|00\rangle) + 2\,\text{QFT}(|01\rangle) + 3\,\text{QFT}(|10\rangle) + 4\,\text{QFT}(|11\rangle)) \tag{A6}$$

Here, amplitude encodes pixel intensity. The Equations (A5) and (A6) show that QFT operates on position qubits, converting spatial information into frequency components. FTQR enables frequency-domain operations but may reduce spatial reconstruction accuracy relative to purely spatial methods.

Appendix A.5. QUALPI Example

Consider a 2×2 grayscale image with normalized pixel intensities:

$$I = \begin{bmatrix} 0.0 & 0.5 \\ 0.75 & 1.0 \end{bmatrix}$$

Assign position qubits: $|00\rangle, |01\rangle, |10\rangle, |11\rangle$. Using QUALPI, the pixel intensities are compressed into fewer qubits, e.g., mapping each intensity to a 1-qubit compressed state:

$$|C_0\rangle = |0\rangle, \quad |C_1\rangle = |+\rangle, \quad |C_2\rangle = |-\rangle, \quad |C_3\rangle = |1\rangle \tag{A7}$$

The quantum state is

$$|\Psi_{\text{QUALPI}}\rangle = |00\rangle \otimes |0\rangle + |01\rangle \otimes |+\rangle + |10\rangle \otimes |-\rangle + |11\rangle \otimes |1\rangle \tag{A8}$$

Here, position qubits encode the spatial coordinates (x, y). Compressed qubits encode intensity in a reduced form to save qubits. QUALPI improves storage and qubit efficiency, but it may lose some intensity fidelity during reconstruction [2,15].

Appendix A.6. QRMW Example

Consider a 2×2 spatial image with 2 wavelengths (λ_0, λ_1) and normalized pixel intensities:

$$I_{\lambda_0} = \begin{bmatrix} 0.0 & 0.5 \\ 0.75 & 1.0 \end{bmatrix}, \quad I_{\lambda_1} = \begin{bmatrix} 1.0 & 0.25 \\ 0.5 & 0.75 \end{bmatrix}$$

Assign position qubits: $|00\rangle, |01\rangle, |10\rangle, |11\rangle$, and wavelength qubits: $|\lambda_0\rangle = |0\rangle, |\lambda_1\rangle = |1\rangle$. The QRMW quantum image representation is defined in Equation (A9).

$$\begin{aligned} |\Psi_{\text{QRMW}}\rangle = & |0\rangle \otimes |00\rangle \otimes |0\rangle + |0.5\rangle \otimes |01\rangle \otimes |0\rangle \\ & + |0.75\rangle \otimes |10\rangle \otimes |0\rangle + |1.0\rangle \otimes |11\rangle \otimes |0\rangle \\ & + |1.0\rangle \otimes |00\rangle \otimes |1\rangle + |0.25\rangle \otimes |01\rangle \otimes |1\rangle \\ & + |0.5\rangle \otimes |10\rangle \otimes |1\rangle + |0.75\rangle \otimes |11\rangle \otimes |1\rangle \end{aligned} \tag{A9}$$

Here, intensity qubits encode pixel intensity for each wavelength. The next two qubits encode spatial coordinates (x, y). The last qubit encodes wavelength. QRMW enables multi-wavelength image representation, but it increases qubit count and circuit complexity, which may limit scalability on NISQ devices [2,3].

Appendix A.7. EBA-QR & SA-QIR Example

Consider a 2×2 grayscale image with normalized pixel intensities:

$$\begin{bmatrix} 0.25 & 0.25 \\ 0.25 & 0.25 \end{bmatrix} \tag{A10}$$

In EBA-QR, pixel intensities are treated as probabilities to compute global entropy:

$$p_0 = p_1 = p_2 = p_3 = 0.25 \tag{A11}$$

The image entropy is calculated as

$$H = -\sum_{i=0}^{3} p_i \log_2 p_i = -4 \cdot 0.25 \cdot \log_2 0.25 = 2 \text{ bits} \tag{A12}$$

In a quantum circuit, this entropy information can guide amplitude encoding or structural feature encoding:

$$|\Psi_{\text{EBA-QR}}\rangle = \sum_{x,y} \sqrt{p_{x,y}} \, |x, y\rangle \tag{A13}$$

For our 2×2 example:

$$|\Psi_{\text{EBA-QR}}\rangle = \frac{1}{2}\left(|00\rangle + |01\rangle + |10\rangle + |11\rangle\right) \tag{A14}$$

Here, qubits encode global pixel distribution probabilities rather than exact intensities. This representation captures statistical and structural information effectively, but it does not preserve exact pixel intensities. It is suitable for pattern recognition, feature extraction, or texture analysis, rather than precision imaging [2,8].

Appendix A.8. EFRQIs Example

Consider a 2×2 grayscale image with normalized pixel intensities:

$$\begin{bmatrix} 0.0 & 0.5 \\ 0.75 & 1.0 \end{bmatrix} \tag{A15}$$

The amplitude coefficients are computed as

$$\alpha_{x,y} = \cos\left(\frac{\pi}{2} p_{x,y}\right), \quad \beta_{x,y} = \sin\left(\frac{\pi}{2} p_{x,y}\right) \tag{A16}$$

Thus, for each pixel:

$$\begin{aligned} &(0,0) : \alpha_{0,0} = 1, \quad \beta_{0,0} = 0 \\ &(0,1) : \alpha_{0,1} \approx 0.707, \quad \beta_{0,1} \approx 0.707 \\ &(1,0) : \alpha_{1,0} \approx 0.383, \quad \beta_{1,0} \approx 0.924 \\ &(1,1) : \alpha_{1,1} = 0, \quad \beta_{1,1} = 1 \end{aligned} \tag{A17}$$

The 2×2 EFRQIs quantum state is then:

$$\begin{aligned} |\Psi_{\text{EFRQI}}\rangle = &\alpha_{0,0}|0\rangle \otimes |00\rangle + \alpha_{0,1}|0\rangle \otimes |01\rangle + \alpha_{1,0}|0\rangle \otimes |10\rangle \\ &+ \alpha_{1,1}|0\rangle \otimes |11\rangle + \beta_{0,0}|1\rangle \otimes |00\rangle + \beta_{0,1}|1\rangle \otimes |01\rangle \\ &+ \beta_{1,0}|1\rangle \otimes |10\rangle + \beta_{1,1}|1\rangle \otimes |11\rangle \end{aligned} \tag{A18}$$

Equations (A17) and (A18) show that the first qubit encodes pixel intensity probabilistically using amplitudes $(\alpha_{x,y}, \beta_{x,y})$. The final 2 qubits contain pixel coordinates (x, y). EFRQIs minimizes the distortion of intensity when compared to FRQIs; however, it is probabilistic with possible residual reconstruction errors [2,3]. Unlike EFRQI-based [9] approaches that primarily rely on amplitude encoding, the proposed IP-QIR framework introduces a hybrid encoding mechanism combining intensity-based representation with adaptive entropy-driven compression. This allows improved flexibility in encoding and better suitability for resource-constrained quantum systems.

References

1. Yan, F.; Iliyasu, A.M.; Jiang, Z. Quantum computation-based image representation, processing operations and their applications. *Entropy* **2014**, *16*, 5290–5338. [CrossRef]
2. Mastriani, M.; Iyengar, S.S.; Kumar, L. Analysis of five techniques for the internal representation of a digital image inside a quantum processor. *SN Comput. Sci.* **2021**, *2*, 450. [CrossRef]
3. Farooq, U.; Singh, P.; Kumar, A. A systematic review of quantum image processing: Representation, applications and future perspectives. *Comput. Sci. Rev.* **2025**, *57*, 100763. [CrossRef]
4. Su, J.; Guo, X.; Liu, C.; Li, L. An improved novel quantum image representation and its experimental test on IBM quantum experience. *Sci. Rep.* **2021**, *11*, 13879. [CrossRef] [PubMed]
5. Cai, Y.; Lu, X.; Jiang, N. A survey on quantum image processing. *Chin. J. Electron.* **2018**, *27*, 718–727. [CrossRef]
6. Chakraborty, S.; Mandal, S.; Shaikh, S. Quantum image processing: Challenges and future research issues. *arXiv* **2020**, arXiv:2008.12983. [CrossRef]
7. Yan, F.; Iliyasu, A.M.; Venegas-Andraca, S.E. A survey of quantum image representations. *Quantum Inf. Process.* **2016**, *15*, 1–35. [CrossRef]
8. Wang, Z. Review of quantum image processing. *Arch. Comput. Methods Eng.* **2019**, *26*, 769–786. [CrossRef]
9. Haque, M.E.; Paul, M.; Ulhaq, A.; Debnath, T. Advanced quantum image representation and compression using a DCT-EFRQI approach. *Sci. Rep.* **2023**, *13*, 4129. [CrossRef]
10. Jiang, N.; Wang, J.; Mu, Y. Quantum image scaling up based on nearest-neighbor interpolation. *Quantum Inf. Process.* **2015**, *14*, 4001–4026. [CrossRef]
11. Song, X.; Wang, S.; Liu, S. A dynamic watermarking scheme for quantum images using quantum wavelet transform. *Quantum Inf. Process.* **2013**, *12*, 3689–3706. [CrossRef]
12. Yuan, S.; Mao, X.; Li, T.; Xue, Y.; Chen, L.; Xiong, Q. Quantum morphology operations based on quantum representation model. *Quantum Inf. Process.* **2015**, *14*, 1625–1645. [CrossRef]

13. Zhou, N.R.; Hua, T.X.; Gong, L.H.; Pei, D.J.; Liao, Q.H. Quantum image encryption based on generalized Arnold transform and double random-phase encoding. *Quantum Inf. Process.* **2015**, *14*, 1193–1213. [CrossRef]
14. Hu, B.; Huang, X.; Zhou, R.; Wei, Y.; Wan, Q.; Pang, C. A theoretical framework for quantum image representation and data loading scheme. *Sci. China Inf. Sci.* **2014**, *57*, 032108. [CrossRef]
15. Deb, S.K.; Pan, W.D. Quantum image compression: Fundamentals, algorithms, and advances. *Computers* **2024**, *13*, 187. [CrossRef]
16. Geng, A.; Moghiseh, A.; Redenbach, C.; Schladitz, K. Improved FRQI on superconducting processors and its restrictions in the NISQ era. *Quantum Inf. Process.* **2023**, *22*, 104. [CrossRef]
17. Le, P.Q.; Dong, F.; Hirota, K. A flexible representation of quantum images for polynomial preparation, image compression, and processing operations. *Quantum Inf. Process.* **2011**, *10*, 63–84. [CrossRef]
18. Venegas-Andraca, S.E. Quantum walks: A comprehensive review. *Quantum Inf. Process.* **2012**, *11*, 1015–1106. [CrossRef]
19. Grigoryan, A.M.; Gomez, A.; Agaian, S.S.; Panetta, K. Quantum edge detection and convolution using paired transform-based image representation. *Information* **2025**, *16*, 255. [CrossRef]
20. Niu, X.; Song, X.H.; Wang, S. Multi-channel quantum image representation based on phase transform and elementary transformations. *J. Inf. Hiding Multimed. Signal Process.* **2014**, *5*, 574–585.
21. Li, K.; Zhang, Y.; Lü, K.; Wang, X.; Wang, X. An optimized quantum representation for color digital images. *Int. J. Theor. Phys.* **2018**, *57*, 2938–2948. [CrossRef]
22. Preskill, J. Quantum computing in the NISQ era and beyond. *Quantum* **2018**, *2*, 79. [CrossRef]
23. Bharti, K.; Cervera-Lierta, A.; Kyaw, T.H.; Haug, T.; Alperin-Lea, S.; Anand, A.; Degroote, M.; Heimonen, H.; Kottmann, J.S.; Menke, T.; et al. Noisy intermediate-scale quantum algorithms. *Rev. Mod. Phys.* **2022**, *94*, 015004. [CrossRef]
24. Alam, M.; Ash-Saki, A.A.; Ghosh, S. An efficient circuit compilation flow for quantum approximate optimization algorithm. In *Proceeding of the 2020 57th ACM/IEEE Design Automation Conference (DAC), San Francisco, CA, USA, 20–24 July 2020*; IEEE: Piscataway, NJ, USA, 2020; pp. 1–6. [CrossRef]
25. Zheng, K.; Li, K.; Cong, S. A reconstruction algorithm for compressive quantum tomography using various measurement sets. *Sci. Rep.* **2016**, *6*, 38497. [CrossRef]
26. Lohani, S.; Kirby, B.T.; Brodsky, M.; Danaci, O.; Glasser, R.T. Machine learning assisted quantum state estimation with improved fidelity. *arXiv* **2020**, arXiv:2003.03441.
27. Yan, F.; Huang, H.; Pedrycz, W.; Hirota, K. Review of medical image processing using quantum-enabled algorithms. *Artif. Intell. Rev.* **2024**, *57*, 300. [CrossRef]
28. Yousif, S.; Al-Khateeb, B.; Garcia-Zapirain, B. A new quantum circuits of quantum convolutional neural network for X-ray image classification. *IEEE Access* **2024**, *12*, 65660–65671. [CrossRef]
29. Cruz, H. A review of synthetic-aperture radar image formation algorithms. *Remote Sens.* **2022**, *14*, 1258. [CrossRef]
30. Miller, L.; Uehara, G.; Sharma, A.; Spanias, A. Quantum image fusion methods for remote sensing. In *Proceedings of the 2024 IEEE Aerospace Conference, Big Sky, MT, USA, 2–9 March 2024*; IEEE: Piscataway, NJ, USA, 2024; pp. 1–9. [CrossRef]
31. Stoudenmire, E.M.; Schwab, D.J. Supervised learning with tensor networks. In Proceedings of the 30th International Conference on Neural Information Processing Systems (NeurIPS), Barcelona, Spain, 5–10 December 2016; NeurIPS Foundation: San Diego, CA, USA; pp. 4799–4807.
32. Nielsen, M.A.; Chuang, I.L. *Quantum Computation and Quantum Information*; Cambridge University Press: Cambridge, UK, 2010.
33. Willsch, M.; Willsch, D.; Jin, F.; De Raedt, H.; Michielsen, K. Benchmarking the quantum approximate optimization algorithm. *Quantum Inf. Process.* **2020**, *19*, 197. [CrossRef]
34. McClean, J.R.; Romero, J.; Babbush, R.; Aspuru-Guzik, A. The theory of variational hybrid quantum-classical algorithms. *New J. Phys.* **2016**, *18*, 023023. [CrossRef]
35. Schuld, M.; Killoran, N. Is quantum advantage the right goal for quantum machine learning? *PRX Quantum* **2022**, *3*, 030101. [CrossRef]
36. Cerezo, M.; Verdon, G.; Huang, H.-Y.; Cincio, L.; Coles, P.J. Challenges and opportunities in quantum machine learning. *Nat. Comput. Sci.* **2022**, *2*, 567–576. [CrossRef]
37. Stein, S.A.; Wiebe, N.O.; Ang, J.A.; Li, A. Benchmarking quantum processor performance through quantum distance metrics. In *Proceedings of the 2022 IEEE International Parallel and Distributed Processing Symposium Workshops (IPDPSW), Lyon, France, 30 May–3 June 2022*; IEEE: Piscataway, NJ, USA, 2022; pp. 618–624. [CrossRef]
38. Liu, Y.-H.; Qi, Z.-D.; Liu, Q. Comparison of the similarity between two quantum images. *Sci. Rep.* **2022**, *12*, 7776. [CrossRef]
39. Srivastava, M.; Moulick, S.K.; Panigrahi, P.K. Quantum image representation through 2D states. *arXiv* **2013**, arXiv:1305.2251. [CrossRef]
40. Erkan, Z.; Rahebi, J.; Yelghi, A. Quantum image dataset transform (QIDT) for image processing. *Quantum Inf. Process.* **2025**, *24*, 156. [CrossRef]
41. Xiao, Y.; Fonov, V.; Chakravarty, M.M.; Beriault, S.; Al Subaie, F.; Sadikot, A.; Pike, G.B.; Bertrand, G.; Collins, D.L. A dataset of multi-contrast population-averaged brain MRI atlases of a Parkinson's disease cohort. *Data Brief* **2017**, *12*, 370–379. [CrossRef]

42. Georgescu, I.M.; Ashhab, S.; Nori, F. Quantum simulation. *Rev. Mod. Phys.* **2014**, *86*, 153. [CrossRef]
43. Sheikh, H.R.; Sabir, M.F.; Bovik, A.C. A statistical evaluation of recent full reference image quality assessment algorithms. *IEEE Trans. Image Process.* **2006**, *15*, 3440–3451. [CrossRef]
44. Sugunapriya, A.; Markkandan, S. Variational quantum enhanced deep transfer learning for small underwater aqua species image classification. *Sci. Rep.* **2025**, *15*, 38551. [CrossRef] [PubMed]
45. Duan, L.; Wang, J.; Qiao, S.; Ma, B. Quantum image representation methods: A survey and future directions. *Inf. Fusion* **2022**, *79*, 149–167. [CrossRef]
46. Fonov, V.S.; Evans, A.C.; Botteron, K.; Almli, C.R.; McKinstry, R.C.; Collins, D.L.; Brain Development Cooperative Group. Unbiased average age-appropriate atlases for pediatric studies. *NeuroImage* **2011**, *54*, 313–327. [CrossRef]
47. Qiskit Development Team. Qiskit: An open-source framework for quantum computing. *Zenodo* **2024**. [CrossRef]
48. Eisert, J.; Hangleiter, D.; Walk, N.; Roth, I.; Markham, D.; Parekh, R.; Chabaud, U.; Kashefi, E. Quantum certification and benchmarking. *Nat. Rev. Phys.* **2020**, *2*, 382–390. [CrossRef]
49. Larson, E.C.; Chandler, D.M. Most apparent distortion: Full-reference image quality assessment and the role of strategy. *J. Electron. Imaging* **2010**, *19*, 011006. [CrossRef]
50. Coppersmith, D. An approximate Fourier transform useful in quantum factoring. *arXiv* **2002**, arXiv:quant-ph/0201067. [CrossRef]
51. Kim, S. Scalable feed-forward and backward quantum image representation based on stereographic projection. *Eng. Appl. Artif. Intell.* **2026**. [CrossRef]
52. Madge, V.; Fonov, V.S.; Xiao, Y.; Zou, L.; Jackson, C.; Postuma, R.B.; Dagher, A.; Fon, E.A.; Collins, D.L. A dataset of multi-contrast unbiased average MRI templates of a Parkinson's disease population. *medRxiv* **2022**. [CrossRef]
53. Shende, V.V.; Bullock, S.S.; Markov, I.L. Synthesis of quantum-logic circuits. *IEEE Trans. Comput.-Aided Des. Integr. Circuits Syst.* **2006**, *25*, 1000–1010. [CrossRef]
54. Devitt, S.J.; Munro, W.J.; Nemoto, K. Quantum error correction for beginners. *Rep. Prog. Phys.* **2013**, *76*, 076001. [CrossRef]
55. Wien, M. *High Efficiency Video Coding: Coding Tools and Specification*; Springer: Berlin/Heidelberg, Germany, 2015. [CrossRef]
56. Biamonte, J.; Wittek, P.; Pancotti, N.; Rebentrost, P.; Wiebe, N.; Lloyd, S. Quantum machine learning. *Nature* **2017**, *549*, 195–202. [CrossRef]
57. Montanaro, A. Quantum algorithms: An overview. *npj Quantum Inf.* **2016**, *2*, 15023. [CrossRef]
58. Dale, A.M.; Fischl, B.; Sereno, M.I. Cortical surface-based analysis: I. Segmentation and surface reconstruction. *NeuroImage* **1999**, *9*, 179–194. [CrossRef] [PubMed]
59. Horodecki, R.; Horodecki, P.; Horodecki, M.; Horodecki, K. Quantum entanglement. *Rev. Mod. Phys.* **2009**, *81*, 865–942. [CrossRef]
60. IBM Quantum. IBM Quantum System Two: Advancing quantum computing with 127+ qubit processors. *IBM Res.* **2024**. Available online: https://www.ibm.com/quantum (accessed on 13 April 2026).
61. Zhang, Y.; Lu, K.; Gao, Y.; Wang, M. NEQR: A novel enhanced quantum representation of digital images. *Quantum Inf. Process.* **2013**, *12*, 2833–2860. [CrossRef]
62. Khandelwal, A.; Chandra, M.G.; Pramanik, S. On classifying images using quantum image representation. In *Proceedings of the 2022 IEEE/ACM 7th Symposium on Edge Computing (SEC), Seattle, WA, USA, 5–8 December 2022*; IEEE: Piscataway, NJ, USA, 2022; pp. 444–449. [CrossRef]
63. Li, H.-S.; Chen, X.; Xia, H.; Liang, Y.; Zhou, Z. A quantum image representation based on bitplanes. *IEEE Access* **2018**, *6*, 62396–62404. [CrossRef]
64. Mandal, A.; Banerjee, S.; Panigrahi, P.K. Quantum image representation on clusters. In *Proceedings of the 2021 IEEE International Conference on Quantum Computing and Engineering (QCE), Broomfield, CO, USA, 17–22 October 2021*; IEEE: Piscataway, NJ, USA, 2021; pp. 89–99. [CrossRef]
65. Haque, M.E.; Paul, M.; Tohidi, F.; Ulhaq, A.; Debnath, T. Enhancing image representation and compression: An innovative NZ-NQER framework with block truncation quantum coding. In *Proceedings of the International Conference on Digital Image Computing: Techniques and Applications (DICTA), Port Macquarie, Australia, 28 November–1 December 2023*; IEEE: Piscataway, NJ, USA, 2023; pp. 304–311. [CrossRef]
66. Boreiri, Z.; Azad, A.N.; Majd, N. Optimized quantum circuits in quantum image processing using Qiskit. In *Proceedings of the 2022 International Conference on Machine Vision and Image Processing (MVIP), Ahvaz, Iran, 23–24 February 2022*; IEEE: Piscataway, NJ, USA, 2022; pp. 1–7. [CrossRef]
67. Hammou, I.; Ziet, L.; Kouadra, I.; Abdelhalim, B. Comparison between FRQI and NEQR representation. In *Proceedings of the 2024 International Conference on Advances in Electrical and Communication Technologies (ICAECOT), Setif, Algeria, 1–3 October 2024*; IEEE: Piscataway, NJ, USA, 2024; pp. 1–6. [CrossRef]
68. Tiwari, A.; Sakhuja, S.; Britant. Benchmarking quantum image representation algorithms for hybrid-quantum applications. In *Proceedings of the 2025 17th International Conference on COMmunication Systems and NETworks (COMSNETS), Bengaluru, India, 6–10 January 2025*; IEEE: Piscataway, NJ, USA, 2025; pp. 1108–1113. [CrossRef]

69. Singh, B.; Indu, S.; Majumdar, S. Development of a classification architecture for images represented using quantum theory using IBM Qiskit libraries. In *Proceedings of the 2023 3rd International Conference on Artificial Intelligence and Signal Processing (AISP), Vijayawada, India, 18–20 March 2023*; IEEE: Piscataway, NJ, USA, 2023; pp. 1–5. [CrossRef]
70. Grigoryan, A.M.; Agaian, S.S. Conclusion and opportunities and challenges of quantum image processing. In *Quantum Image Processing in Practice: A Mathematical Toolbox*; Wiley: Hoboken, NJ, USA, 2025; pp. 285–289. [CrossRef]
71. Haque, M.E.; Paul, M.; Ulhaq, A.; Debnath, T. A novel state connection strategy for quantum computing to represent and compress digital images. In *Proceedings of the ICASSP 2023-2023 IEEE International Conference on Acoustics, Speech and Signal Processing (ICASSP), Rhodes Island, Greece, 4–10 June 2023*; IEEE: Piscataway, NJ, USA, 2023; pp. 1–5. [CrossRef]
72. Xing, Z.; Lam, C.-T.; Yuan, X.; Im, S.-K.; Machado, P. MMQW: Multi-modal quantum watermarking scheme. *IEEE Trans. Inf. Forensics Secur.* **2024**, *19*, 5181–5195. [CrossRef]
73. LaRose, R.; Tikku, A.; O'Neel-Judy, É.; Cincio, L.; Coles, P.J. Variational quantum state diagonalization. *npj Quantum Inf.* **2019**, *5*, 57. [CrossRef]
74. RequieMonk. Sentinel-1 and Sentinel-2 Image Pairs Segregated by Terrain. Kaggle 2022. Available online: https://www.kaggle.com/datasets/requiemonk/sentinel12-image-pairs-segregated-by-terrain (accessed on 13 April 2026).
75. Rahman, T. Tuberculosis (TB) Chest X-Ray Dataset. Kaggle 2022. Available online: https://www.kaggle.com/datasets/tawsifurrahman/tuberculosis-tb-chest-xray-dataset (accessed on 13 April 2026).
76. Guo, H.; Sun, C.; Zhang, J.; Zhang, W.; Zhang, N. MMYFNet: Multi-modality YOLO fusion network for object detection in remote sensing images. *Remote Sens.* **2024**, *16*, 4451. [CrossRef]
77. Silva, R.; Coelho, E.; Pimenta, N.; Durães, D.; Alves, V.; Bandeira, L.; Machado, J.; Novais, P.; Melo-Pinto, P. Multimodal object detection: An architecture using feature-level fusion and deep learning. *Neural Comput. Appl.* **2025**, *37*, 23799–23810. [CrossRef]
78. Mi, Y.; Chi, M.; Zhang, Q.; Liu, P. Research on multi-scale fusion image enhancement and improved YOLOv5s lightweight detection. *Sci. Rep.* **2024**, *14*, 28280. [CrossRef]
79. Zhao, Z.; Bai, H.; Zhang, J.; Zhang, Y.; Xu, S.; Lin, Z.; Van Gool, L. Correlation-driven dual-branch feature decomposition for multi-modality image fusion. *arXiv* **2022**, arXiv:2211.14461. [CrossRef]
80. Wang, Y.; Sun, H.; Wang, X.; Zhang, B.; Li, C.; Xin, Y.; Ding, E.; Han, S. MAFormer: A transformer network with multi-scale attention fusion for visual recognition. *arXiv* **2022**, arXiv:2209.01620. [CrossRef]
81. Dai, Y.; Gieseke, F.; Oehmcke, S.; Wu, Y.; Barnard, K. Attentional feature fusion. *arXiv* **2020**, arXiv:2009.14082. [CrossRef]
82. He, Y.; Xi, B.; Li, G.; Zheng, T.; Li, Y.; Xue, C.; Chanussot, J. Multilevel attention dynamic-scale network for hyperspectral and LiDAR data fusion classification. *IEEE Trans. Geosci. Remote Sens.* **2024**, *62*, 1–16. [CrossRef]
83. Chen, X.; Liu, Z.-H.; Chen, H.-W.; Xu, C.-Z. QIPC: A Novel Quantum Image Representation Model for Polar Coordinate Images. *Quantum Inf. Process.* **2021**, *21*, 174. [CrossRef]
84. Alsubai, S.; Alqahtani, A.; Binbusayyis, A.; Sha, M.; Gumaei, A.; Wang, S. A quantum computing-based accelerated model for image classification using a parallel pipeline encoded inception module. *Mathematics* **2023**, *11*, 2513. [CrossRef]
85. Amankwah, M.G.; Camps, D.; Van Beeumen, R. Quantum pixel representations for multi-dimensional images. *Sci. Rep.* **2022**, *12*, 7712. [CrossRef] [PubMed]
86. Zhang, J.; Zhang, Y.; Zhou, Y. Quantum-Inspired Spectral-Spatial Pyramid Network for Hyperspectral Image Classification. In *Proceedings of the IEEE/CVF Conference on Computer Vision and Pattern Recognition (CVPR), Vancouver, BC, Canada, 18–22 June 2023*; IEEE: Piscataway, NJ, USA, 2023; pp. 9925–9934. [CrossRef]
87. Yu, X.; Tian, X. A fault detection algorithm based on immune neural network for pipeline monitoring. *Int. J. Press. Vessel. Pip.* **2022**, 104611. [CrossRef]
88. Qin, H.; Huang, X.; Wang, X.; Zhou, Z. Identification and classification of oil and gas pipeline intrusion events using CNN. *PLoS ONE* **2025**, *20*, e0338205. [CrossRef]
89. Verma, P.; Gandhi, K.; Cheema, A.M.; Ashfaq, M.; Shah, D.; Ali, S.; Tahir, M. DeepPipeNet: Deep learning-based anomaly detection for pipeline monitoring. *Discov. Appl. Sci.* **2026**, *8*, 520. [CrossRef]

Disclaimer/Publisher's Note: The statements, opinions and data contained in all publications are solely those of the individual author(s) and contributor(s) and not of MDPI and/or the editor(s). MDPI and/or the editor(s) disclaim responsibility for any injury to people or property resulting from any ideas, methods, instructions or products referred to in the content.